

---

# StAD: Stein Amortized Divergence for Fast Likelihoods with Diffusion and Flow

---

Gurjeet Jagwani<sup>1,2</sup> Stephen Thorp<sup>1</sup> Sinan Deger<sup>1</sup> Hiranya Peiris<sup>1,3,4</sup>

## Abstract

Diffusion and flow-based models are ubiquitously used for generative modelling and density estimation. They admit a deterministic probability flow ordinary differential equation (PF-ODE), analogous to continuous normalizing flows (CNFs), which describes the transport of the probability mass. Obtaining the likelihood from these models is of interest to many workflows, especially Bayesian analysis, and requires solving the trace of the Jacobian to compute the divergence of the learned PF-ODE, which is either  $\mathcal{O}(D^2)$  to compute exactly or  $\mathcal{O}(D)$  with a noisy estimate. We introduce *StAD*, a new distillation method to predict and learn the divergence of the PF-ODE using the Langevin-Stein operator without ever computing the Jacobian. We show that our method is competitive with the Hutchinson and Hutch++ on CIFAR-10, ImageNet and other density estimation tasks, consistently improving the variance and speed of the likelihood predictions compared to the Hutchinson. We additionally show our method will generalize to a varied class of generative models, and show that under some regularity conditions these learned vector fields can be made to satisfy the Stein class.

## 1. Introduction

Density estimation is of great interest to many domains like molecular dynamics, neuroscience, cosmology, astrophysics, materials science, evolutionary biology, economics, simulation-based inference, and reinforcement learning among others (e.g. Arnaudon et al., 2017; Noé et al., 2019;

<sup>1</sup>Institute of Astronomy and Kavli Institute for Cosmology, University of Cambridge, Cambridge, UK <sup>2</sup>Research Computing Services, University of Cambridge, Cambridge, UK <sup>3</sup>Cavendish Laboratory, Department of Physics, University of Cambridge, Cambridge, UK <sup>4</sup>The Oskar Klein Centre, Department of Physics, Stockholm University, Stockholm, SE. Correspondence to: Gurjeet Jagwani <gurjeet.jagwani@ast.cam.ac.uk>.

Alsing et al., 2019; Schebek et al., 2025). Diffusion (Sohl-Dickstein et al., 2015; Song & Ermon, 2019; 2020; Ho et al., 2020; Song et al., 2021b;a) and flow-matching (Lipman et al., 2023; 2024) models are the current state-of-the-art algorithms for estimating the high-dimensional densities commonly encountered within many scientific and non-scientific datasets (for a review, see Yang et al., 2023; Arruda et al., 2025). They fulfil a similar role as other probabilistic models such as normalizing flows (reviewed in Kobyzev et al., 2021; Papamakarios et al., 2021), and build on earlier pioneering work on score-based models (e.g. Hyvärinen, 2005; Vincent, 2011).

### 1.1. Divergence under diffusion and flow

Diffusion and flow-based models are concerned with learning a probability density  $p(\mathbf{x})$  over a variable  $\mathbf{x}$  in  $\mathbb{R}^D$ . This is represented as a continuous-time transform between the target density  $p_\varepsilon(\mathbf{x}_\varepsilon)$  at time  $t = \varepsilon \gtrsim 0$ , and a simple base (noise) density  $p_T(\mathbf{x}_T)$  at time  $t = T$ . Diffusion models learn the score  $\mathbf{s}(\mathbf{x}_t) = \nabla \log p(\mathbf{x}_t)$  of the changing probability density function, with a stochastic differential equation (SDE) guiding this process (Song et al., 2021b). Flow-matching models learn a conditional vector field that is analogous to the marginal vector field describing the transport of the probability mass from noise to data (Lipman et al., 2023). They both can be interpreted as continuous normalising flows (CNFs; Chen et al., 2018a; Grathwohl et al., 2019), or a probability flow ordinary differential equation (PF-ODE; Song et al., 2021b). For both classes of models, the PF-ODE has a general form:

$$\frac{d\mathbf{x}_t}{dt} = \mathbf{v}_t(\mathbf{x}_t), \quad t \in [\varepsilon, T], \quad (1)$$

where  $\mathbf{v}_t$  is any vector field or differential equation describing the transport of probability. In diffusion models—obeying an Itô SDE of the form  $d\mathbf{x}_t = \mathbf{f}(\mathbf{x}_t, t)dt + g(t)d\mathbf{w}$ , where  $\mathbf{f}$  and  $g$  are *drift* and *diffusion* coefficients, and  $\mathbf{w}$  follows a Weiner process—the PF-ODE has the form  $\mathbf{v}_t(\mathbf{x}_t) = \mathbf{f}(\mathbf{x}_t, t) - \frac{1}{2}g(t)^2\mathbf{s}(\mathbf{x}_t)$  (see Maoutsa et al., 2020; Song et al., 2021b). Flow-matching models admit a simulation-free objective to directly approximate  $\mathbf{v}_t$ . The instantaneous change-of-variables formula from CNFs (Chen

et al., 2018a; Grathwohl et al., 2019) gives

$$\frac{d}{dt} \log p_t(\mathbf{x}_t) = -\langle \nabla, \mathbf{v}_t(\mathbf{x}_t) \rangle. \quad (2)$$

Integrating (2) for  $t = T$  to  $t = \varepsilon$  (as in Song et al., 2021b) allows one to compute the log probability (likelihood) of a variable under the target density,

$$\log p_\varepsilon(\mathbf{x}_\varepsilon) = \log p_T(\mathbf{x}_T) + \int_\varepsilon^T \langle \nabla, \mathbf{v}_t(\mathbf{x}_t) \rangle dt, \quad (3)$$

using an initial value  $\mathbf{x}_t = \mathbf{x}_\varepsilon$  at  $t = \varepsilon$ , and simultaneously solving (1) for  $\mathbf{x}_T$ . The bottleneck here is the divergence term—normally computed using the trace of the Jacobian  $\langle \nabla, \mathbf{v}_t(\mathbf{x}_t) \rangle = \text{Tr}(\partial \mathbf{v}_t / \partial \mathbf{x}_t)$ —which is of the time complexity  $\mathcal{O}(D^2)$  to determine exactly, or  $\mathcal{O}(D)$  to approximate using noisy unbiased trace estimators like Hutchinson (Hutchinson, 1989; Skilling, 1989; Girard, 1989; Grathwohl et al., 2019) or Hutch++ (Meyer et al., 2021; Liu et al., 2025). Fig. 1 illustrates an example PF-ODE vector field, and the corresponding divergence scalar field, at a single time step.

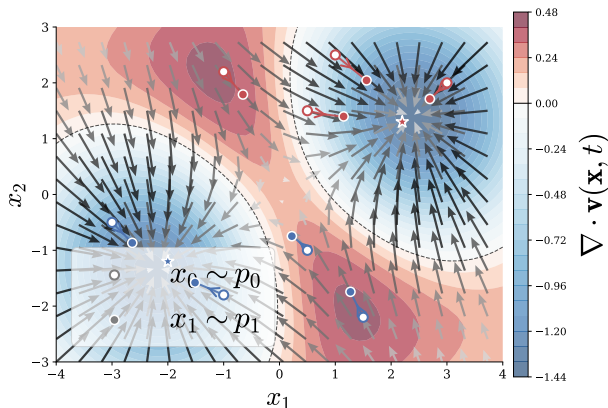


Figure 1. Divergence (blue/red contours) visualisation for a vector field (arrows) defined by the PF-ODE at a fixed time step.

## 1.2. Stein’s method and Stein operators

Stein’s method (Stein, 1972) was introduced to bound the distance between a sum of random variables and the Gaussian distribution. Since then, it has proved to be a powerful tool for quantifying distances between probability measures and bounding convergence rates in limit theorems (Barbour, 1988), and has been extended considerably beyond its original application (for a review, see Anastasiou et al., 2023). Stein operators  $\mathcal{A}_p$  are defined as linear operators acting on a set of test functions  $\mathcal{U}$ , that follow the Stein identity,

$$\mathbb{E}_{x \sim p}[(\mathcal{A}_p u)(x)] = 0, \quad \forall u \in \mathcal{U}, \quad (4)$$

where  $x$  is a random variable from a target distribution  $p$ .

The Langevin–Stein operator is an extension of this formalism to  $\mathbb{R}^D$ . For any density  $p(\mathbf{x})$  with score  $\mathbf{s}(\mathbf{x}) = \nabla \log p(\mathbf{x})$  and any vector field  $\mathbf{v}(\mathbf{x})$  that is in the Stein class, the Langevin–Stein operator,

$$\mathcal{A}_p \mathbf{v}(\mathbf{x}) = \langle \nabla, \mathbf{v}(\mathbf{x}) \rangle + \langle \mathbf{v}(\mathbf{x}), \mathbf{s}(\mathbf{x}) \rangle, \quad (5)$$

satisfies the Stein identity,

$$\mathbb{E}_{\mathbf{x} \sim p}[\mathcal{A}_p \mathbf{v}(\mathbf{x})] = 0, \quad (6)$$

under mild boundary conditions (Gorham & Mackey, 2015; 2017; Liu et al., 2016); see further details in Appendix A and §3.3. Generalizations of the Langevin–Stein operator exist to encompass broader classes of target function (e.g. the diffusion Stein operator; Gorham et al., 2019).

## 1.3. Outline and contributions

In this work, we show that diffusion and flow-matching models satisfy these boundary conditions with some mild assumptions and derive a novel method—the *Stein amortized divergence* (StAD)—that can learn the divergence of the PF-ODE using the Langevin–Stein operator (5). The learned network can then predict the divergence of the vector field at any given time step and produce likelihoods with  $\mathcal{O}(D)$  time complexity and lower variance than the Hutchinson and Hutch++ estimators.

In §2, we review related methods, including general uses of Stein’s method, other trace estimators, and the distillation of diffusion/flow models. In §3, we derive StAD for diffusion and flow-matching. Additionally, we describe regularisation methods for stable training and satisfying the Stein class. In §4 we show results compared to the Hutchinson and Hutch++ estimators for a range of density estimation problems. We conclude the paper in §5.

## 2. Related work

### 2.1. Recent applications of Stein’s method

Stein’s method has been widely adapted as a distance measure between distributions in computational statistics (e.g. Liu et al., 2016; Barp et al., 2019). It has also been utilised to test the quality of a sample generated from a target distribution under MCMC and variational inference settings (Gorham & Mackey, 2015; 2017; Gorham et al., 2019). Chen et al. (2018b) have further developed methodology to deterministically select data points that yield an accurate approximate representation of the posterior, by minimising the Kernel Stein Discrepancy (KSD; Chwialkowski et al., 2016). Stein thinning has also been introduced to post-process MCMC outputs and correct for bias (Riabiz et al., 2022; Bénard et al., 2023). Additionally, Oates et al. (2016) design control variates for Monte Carlo estimators using

the Stein identity. Recent work has been done to introduce Stein’s method into more modern machine learning frameworks. Liu & Wang (2016) introduce Stein Variational Gradient Descent (SVGD) which allows for Bayesian inference as an optimisation problem using Stein discrepancy (see also Ranganath et al., 2016). More recent work by Grathwohl et al. (2020) shows how Stein discrepancies can be utilised to train and evaluate energy-based models.

## 2.2. Trace estimators and tractable Jacobians

As established before, to compute the divergence of the relevant PF-ODE, we need to compute the trace of the Jacobian. Common approaches to achieve this are the Hutchinson (Hutchinson, 1989; Skilling, 1989; Girard, 1989; Silver & Röder, 1994; Grathwohl et al., 2019) and Hutch++ estimators (Meyer et al., 2021; Liu et al., 2025). Hutchinson introduced a stochastic method to estimate the trace of a  $D \times D$  matrix  $\mathbf{A}$  using random noise vectors or *probes*,  $\mathbf{n} \in \mathbb{R}^D$ , that are Rademacher or Gaussian distributed (for a review, see e.g. Avron & Toledo, 2011; Roosta-Khorasani & Ascher, 2015; Lin et al., 2016; Adams et al., 2018; Jiang et al., 2021). The trace of  $\mathbf{A}$  is then estimated in an unbiased way by averaging over probes:  $\text{Tr}(\mathbf{A}) \approx \mathbb{E}_{\mathbf{n}}[\mathbf{n}^\top \mathbf{A} \mathbf{n}]$ . The Hutch++ algorithm introduced by Meyer et al. (2021) provides comparable performance for positive semi-definite (PSD) matrices with fewer matrix–vector multiplications by using a low-rank projection (see also the work of Lin, 2017; Saibaba et al., 2017; Gambhir et al., 2017; Li & Zhu, 2021). An  $n$ -probe, rank- $n$  implementation of Hutch++ proceeds by first generating random matrices  $\mathbf{S}, \mathbf{G} \in \mathbb{R}^{D \times n}$  each with Rademacher-distributed elements. This is followed by a  $QR$  decomposition,  $\mathbf{Q}\mathbf{R} = \mathbf{A}\mathbf{S}$ , yielding an orthonormal basis  $\mathbf{Q} \in \mathbb{R}^{D \times n}$ . The trace of  $\mathbf{A}$  can then be approximated by

$$\begin{aligned} \text{Tr}(\mathbf{A}) \approx & \text{Tr}(\mathbf{Q}^\top \mathbf{A} \mathbf{Q}) \\ & + \frac{1}{n} \text{Tr}(\mathbf{G}^\top (\mathbf{I} - \mathbf{Q}\mathbf{Q}^\top) \mathbf{A} (\mathbf{I} - \mathbf{Q}\mathbf{Q}^\top) \mathbf{G}), \end{aligned} \quad (7)$$

requiring  $3n$  matrix–vector multiplications.

Persson et al. (2022) presented an adaptive variant of Hutch++, building on the work of Meyer et al. (2021), Jiang et al. (2021), and Gittens & Mahoney (2013). XTrace and XNysTrace, introduced by Epperly et al. (2024), are the latest advancement in trace estimators. These are based on a sum over basic trace estimators, achieving much smaller errors for the same matrix–vector multiplication budget as Hutch++. The XTrace algorithm is also based on Rademacher-distributed random vectors  $\Omega \in \mathbb{R}^{D \times n}$  and a  $QR$  decomposition  $\mathbf{Q}\mathbf{R} = \mathbf{A}\Omega$ , yielding  $\mathbf{Q} \in \mathbb{R}^{D \times n}$ ,  $\mathbf{R} \in \mathbb{R}^{n \times n}$  for  $n \leq D$ . Epperly et al. (2024) derive an efficient trace estimator as an average over  $n$  individual estimators, each depending on  $\mathbf{Q}^\top \mathbf{A} \mathbf{Q}$ , and rows and columns

of  $\mathbf{R}^{-1}$ ,  $\mathbf{Q}^\top \Omega$ , and  $(\mathbf{A}\mathbf{Q})^\top \Omega$ . The resulting estimator requires  $2n$  matrix–vector products. Appendix B performs a comparison of Hutch++ and XTrace for random matrices.

Grathwohl et al. (2019), establish how the Hutchinson can be used to train CNFs with cheap likelihood estimates, and allows for more expressive architectures than the predecessors. Liu et al. (2025) again builds upon this, and replaces the Hutchinson with the Hutch++ estimator, and attempts to make it scaleable by caching the  $\mathbf{Q}$  matrix during computations.

A parallel direction is the development of models with Jacobians that are engineered for tractable trace or determinant estimation. Dinh et al. (2015) design non-linear components for estimating the relevant density, and construct Jacobians that have a determinant that is trivial to compute. Chen & Duvenaud (2019) propose volume-preserving flows by extending Dinh et al. (2015) to continuous flows that would have  $\langle \nabla, \mathbf{v} \rangle = 0$  by construction (see also Toth et al., 2020; Biloš & Günnemann, 2021).

## 2.3. Distillation of diffusion and flow-based models

Diffusion and flow-based models generally solve a neural ODE to transform the initial noise to the target distribution. Solving this system is expensive and requires many steps or evaluations along the trajectory. To enable fast sampling, many distillation techniques have been introduced. Salimans & Ho (2022) introduced progressive distillation to teach a student network to solve the trajectory with less time-steps, Song et al. (2023) introduce consistency models which make time jumps using time-discretization solvers, and Lu & Song (2025) stabilise them by making them follow trigonometric identities. It was observed that having straight paths leads to faster ODE solves, leading to the development of the ReFlow framework (Liu et al., 2023; 2024). Furthermore, score identity distillation techniques, were introduced for diffusion models (Zhou et al., 2024) and were recently extended to flow-matching (Zhou et al., 2025). Other distillation methods for few and 1-step generation have shown that it is relatively easy to learn a student network to reduce inference costs of the teacher (e.g. Luhman & Luhman, 2021; Luo et al., 2023; Yin et al., 2024; Sauer et al., 2025). More recently, Ai et al. (2026) introduced a joint-distillation framework, which can learn the divergence of the continuous neural-ODE using the Hutchinson estimator (for a direct comparison see Appendix C). This allows for fast sampling and few step generation in addition to accurate likelihoods. Similarly, Rehman et al. (2026), construct few-step generators with accurate enough likelihoods for importance sampling.

### 3. Methodology

The Langevin–Stein operator (5), defines the relationship between the divergence  $\langle \nabla, \mathbf{v} \rangle$ , the vector field  $\mathbf{v}$  and the score  $\mathbf{s}$ , in terms of expectations,

$$\mathbb{E}_{\mathbf{x}} \left[ \langle \nabla, \mathbf{v}(\mathbf{x}) \rangle + \langle \mathbf{v}(\mathbf{x}), \mathbf{s}(\mathbf{x}) \rangle \right] = 0. \quad (8)$$

The operator can thus be used to define the average divergence of the vector field,

$$\mathbb{E}_{\mathbf{x}} [\langle \nabla, \mathbf{v}(\mathbf{x}) \rangle] = -\mathbb{E}_{\mathbf{x}} [\langle \mathbf{v}(\mathbf{x}), \mathbf{s}(\mathbf{x}) \rangle], \quad (9)$$

which can be used to define a pointwise Stein baseline,

$$b(\mathbf{x}) := -\langle \mathbf{v}(\mathbf{x}), \mathbf{s}(\mathbf{x}) \rangle, \quad (10)$$

which under the expectation has the property  $\mathbb{E}_{\mathbf{x} \sim p} [b(\mathbf{x})] = \mathbb{E}_{\mathbf{x} \sim p} [\langle \nabla, \mathbf{v}(\mathbf{x}) \rangle]$ . Since we already have an estimate of  $\mathbf{v}(\mathbf{x})$  and  $\mathbf{s}(\mathbf{x})$  with score-based models, this is trivial to compute. It has been shown that the score of flow-matching models can be easily obtained under Gaussian assumptions (e.g. Zheng et al., 2023; Lipman et al., 2024; Zhou et al., 2025); this again allows us to define and compute a cheap baseline that captures the average  $\langle \nabla, \mathbf{v}(\mathbf{x}) \rangle$ . To get a more accurate pointwise estimate, we learn a correction term  $\delta(\mathbf{x})$  at each time step. We can define the pointwise divergence as

$$\langle \nabla, \mathbf{v}(\mathbf{x}) \rangle = b(\mathbf{x}) + r(\mathbf{x}), \quad (11)$$

where  $r(\mathbf{x})$  is the target residual we want to learn with  $\delta(\mathbf{x})$ .

The most direct objective to learn an optimal estimate,  $\delta^*(\mathbf{x})$ , of the divergence residual,  $r(\mathbf{x})$ , would be the  $L^2$  regression:

$$\delta^*(\mathbf{x}) = \arg \min_{\delta} \mathbb{E}_{\mathbf{x}} \left[ (\delta(\mathbf{x}) - r(\mathbf{x}))^2 \right]. \quad (12)$$

Here the target residual,

$$r(\mathbf{x}) := \langle \nabla, \mathbf{v}(\mathbf{x}) \rangle + \langle \mathbf{v}(\mathbf{x}), \mathbf{s}(\mathbf{x}) \rangle = \mathcal{A}_p \mathbf{v}(\mathbf{x}), \quad (13)$$

is unknown because it contains  $\langle \nabla, \mathbf{v}(\mathbf{x}) \rangle$ .

Expanding (12) with the binomial theorem,

$$\begin{aligned} \mathbb{E}_{\mathbf{x}} [(\delta(\mathbf{x}) - r(\mathbf{x}))^2] \\ = \mathbb{E}_{\mathbf{x}} [\delta^2(\mathbf{x})] - 2 \mathbb{E}_{\mathbf{x}} [\delta(\mathbf{x}) r(\mathbf{x})] + \mathbb{E}_{\mathbf{x}} [r^2(\mathbf{x})]. \end{aligned} \quad (14)$$

By the Stein identity and divergence theorem, the mixed term in (14) can be rewritten *without* a dependence on  $\langle \nabla, \mathbf{v} \rangle$ :

$$\mathbb{E}_{\mathbf{x}} [\delta(\mathbf{x}) r(\mathbf{x})] = -\mathbb{E}_{\mathbf{x}} [\langle \nabla \delta(\mathbf{x}), \mathbf{v}(\mathbf{x}) \rangle]. \quad (15)$$

We can show this by rewriting the mixed term as an expectation integral, and using the fact that  $\mathbf{s}(\mathbf{x}) = \nabla \log p(\mathbf{x}) = (\nabla p(\mathbf{x})) / p(\mathbf{x})$ , which gives

$$\begin{aligned} \mathbb{E}_{\mathbf{x}} [\delta(\mathbf{x}) r(\mathbf{x})] \\ = \int_{\mathbb{R}^D} [p(\mathbf{x}) \delta(\mathbf{x}) \langle \nabla, \mathbf{v}(\mathbf{x}) \rangle + \delta(\mathbf{x}) \langle \mathbf{v}(\mathbf{x}), \nabla p(\mathbf{x}) \rangle] d\mathbf{x}. \end{aligned} \quad (16)$$

Using the product rule, we can rewrite (16) as

$$\begin{aligned} \mathbb{E}_{\mathbf{x}} [\delta(\mathbf{x}) r(\mathbf{x})] &= \int_{\mathbb{R}^D} \langle \nabla, p(\mathbf{x}) \delta(\mathbf{x}) \mathbf{v}(\mathbf{x}) \rangle d\mathbf{x} \\ &\quad - \int_{\mathbb{R}^D} p(\mathbf{x}) \langle \nabla \delta(\mathbf{x}), \mathbf{v}(\mathbf{x}) \rangle d\mathbf{x}. \end{aligned} \quad (17)$$

To interpret the first term in (17), we can apply the divergence theorem on the ball  $B_R = \{\mathbf{x} \in \mathbb{R}^D : \|\mathbf{x}\| \leq R\}$ , and then take  $R \rightarrow \infty$ . The divergence integral becomes

$$\begin{aligned} \int_{B_R} \langle \nabla, p(\mathbf{x}) \delta(\mathbf{x}) \mathbf{v}(\mathbf{x}) \rangle d\mathbf{x} \\ = \oint_{\partial B_R} \langle p(\mathbf{x}) \delta(\mathbf{x}) \mathbf{v}(\mathbf{x}), \hat{\mathbf{n}} \rangle dS, \end{aligned} \quad (18)$$

where  $\hat{\mathbf{n}} := \mathbf{x} / \|\mathbf{x}\|$  is the outward unit normal on  $\partial B_R$ , and  $dS$  is the  $(D - 1)$ -dimensional surface measure. For diffusion marginals at  $t \geq \varepsilon$ , and vector fields of at most polynomial growth,  $p(\mathbf{x}) \delta(\mathbf{x}) \mathbf{v}(\mathbf{x})$  decays fast enough that the boundary term vanishes (Liu et al., 2016; Liu & Wang, 2016; Gorham & Mackey, 2017; Barp et al., 2019); i.e.,

$$\lim_{R \rightarrow \infty} \oint_{\partial B_R} \langle p(\mathbf{x}) \delta(\mathbf{x}) \mathbf{v}(\mathbf{x}), \hat{\mathbf{n}} \rangle dS = 0. \quad (19)$$

Then we can simplify (17) to

$$\mathbb{E}_{\mathbf{x}} [\delta(\mathbf{x}) r(\mathbf{x})] = -\mathbb{E}_{\mathbf{x}} [\langle \nabla \delta(\mathbf{x}), \mathbf{v}(\mathbf{x}) \rangle]. \quad (20)$$

Plugging this into (14) shows that the optimization in (12) is equivalent—up to the constant  $\mathbb{E}[r^2(\mathbf{x})]$  that is independent of  $\delta(\mathbf{x})$ —to minimizing the fully *computable* objective

$$L(\delta) = \mathbb{E}_{\mathbf{x}} [\delta^2(\mathbf{x}) + 2 \langle \nabla \delta(\mathbf{x}), \mathbf{v}(\mathbf{x}) \rangle]. \quad (21)$$

$L(\delta)$  uses only samples  $\mathbf{x} \sim p$  and evaluations of the vector field  $\mathbf{v}(\mathbf{x})$ . Its minimizer is  $\delta^*(\mathbf{x}) = \arg \min_{\delta} L(\delta) \approx r(\mathbf{x})$ , so we can approximate the divergence using the learned  $\delta^*(\mathbf{x})$ :

$$\langle \nabla, \mathbf{v}(\mathbf{x}) \rangle \approx \underbrace{b(\mathbf{x}) + \delta^*(\mathbf{x})}_{\text{baseline + residual}}. \quad (22)$$

We will now apply this framework to diffusion models (§3.1), and flow matching/rectified flow models (§3.2).

### 3.1. StAD for diffusion

For a diffusion model indexed by time  $t \in [\varepsilon, T]$ , we can first define a set of instantaneous quantities,

$$\mathbf{s}_t(\mathbf{x}_t) = \nabla \log p_t(\mathbf{x}_t), \quad (23)$$

$$b_t(\mathbf{x}_t) = -\langle \mathbf{v}_t(\mathbf{x}_t), \mathbf{s}_t(\mathbf{x}_t) \rangle, \quad (24)$$

where,  $p_t(\mathbf{x}_t)$  is the marginal density at time  $t$ ,  $\mathbf{v}_t(\mathbf{x}_t)$  is the PF-ODE,  $\mathbf{s}_t(\mathbf{x}_t)$  is the pre-trained score network, and  $b(\mathbf{x}_t)$  is the Stein baseline. We learn a *time-dependent* scalar head  $\delta(\mathbf{x}_t; t)$  to approximate the divergence residual, by averaging the loss in (21) across times. We can define an instantaneous loss,

$$L(\delta; t) = \mathbb{E}_{\mathbf{x}_\varepsilon} \mathbb{E}_{\mathbf{x}_t | \mathbf{x}_\varepsilon} \left[ \delta^2(\mathbf{x}_t; t) + 2 \langle \nabla \delta(\mathbf{x}_t; t), \mathbf{v}_t(\mathbf{x}_t) \rangle \right], \quad (25)$$

as an average over the conditional distribution  $p_t(\mathbf{x}_t | \mathbf{x}_\varepsilon)$  (the noising process, which can be easily sampled in closed form; see e.g. Song et al., 2021b), and the target  $p(\mathbf{x}_\varepsilon)$ . Our total loss will be the time average of this,

$$L(\delta) = \mathbb{E}_t [L(\delta; t)] \quad (26)$$

with  $p(t) = U(\varepsilon, T)$  uniform between  $\varepsilon$  and  $T$  (although see Appendix D). We minimize this loss to find the optimum:  $\delta^*(\mathbf{x}; t) = \arg \min_\delta [L(\delta(\mathbf{x}_t; t))]$ .

At test time, we simply replace  $\langle \nabla, \mathbf{v}_t(\mathbf{x}_t) \rangle$  inside (3) by the learned surrogate  $b_t(\mathbf{x}_t) + \delta^*(\mathbf{x}_t; t)$  and integrate a scalar log-ODE alongside the state ODE from  $t = \varepsilon$  to  $t = T$ ,

$$\frac{d\mathbf{x}_t}{dt} = \mathbf{v}_t(\mathbf{x}_t), \quad \frac{d\ell_t}{dt} = b_t(\mathbf{x}_t) + \delta^*(\mathbf{x}_t; t), \quad (27)$$

with initial values at  $t = \varepsilon$  of  $\mathbf{x}_\varepsilon$  (the known sample whose log likelihood we wish to evaluate) and  $\ell_\varepsilon = 0$ . Solving the two ODEs for  $\mathbf{x}_T$  and  $\ell_T$  gives our log likelihood:

$$\log p_\varepsilon(\mathbf{x}_\varepsilon) \approx \log p_T(\mathbf{x}_T) + \ell_T \quad (28)$$

For a conditional setting, we can follow the same approach as above, but with a context/conditioning variable,  $z$ , introduced. In such a setting,  $\mathbf{v}_t$ ,  $\mathbf{s}_t$ ,  $b$ , and  $\delta$  will all be modified to take  $z$  as an input,  $p(\mathbf{x}_\varepsilon)$  will become  $p(\mathbf{x}_\varepsilon | z)$ , and the loss will be additionally averaged over  $z$ . In both cases, the runtime cost is just forward passes through the velocity field  $\mathbf{v}_t$ , the teacher score  $\mathbf{s}_t$  for  $b_t$ , and the small head  $\delta$ ; no Jacobian traces are needed.

### 3.2. StAD for flow-matching and rectified flows

The obvious challenges to extending *StAD* to other generative models are the availability of a score for the baseline, and ensuring the vector field is of Stein class. Although flow-matching and rectified flow models (Lipman et al.,

2023; Liu et al., 2023) were developed as a different class of models to diffusion, it has been shown recently (Kingma & Gao, 2023; Zhou et al., 2025; Albergo et al., 2025) that flow-matching models are equivalent to diffusion under Gaussian conditions (see also the work of Karras et al., 2022; 2024).

Zhou et al. (2025) define the Gaussian score identity as

$$\mathbf{s}_t(\mathbf{x}_t) = \nabla_{\mathbf{x}_t} \log p_t(\mathbf{x}_t) = -\frac{\mathbf{x}_t - \alpha_t \mathbb{E}[\mathbf{x}_\varepsilon | \mathbf{x}_t]}{\sigma_t^2}, \quad (29)$$

where  $\alpha_t$  and  $\sigma_t$  define the noising schedule, with

$$p(\mathbf{x}_t | \mathbf{x}_\varepsilon) = N(\alpha_t \mathbf{x}_\varepsilon, \sigma_t^2 \mathbf{I}). \quad (30)$$

defining the noising process. The most common configuration is to set  $\alpha_t = 1 - t$  and  $\sigma_t = t$ . The score in (29) is equivalent to Tweedie’s formula (e.g. Robbins, 1992; Efron, 2011). The conditional flow-matching objective (Lipman et al., 2023),

$$\mathcal{L}(\theta) = \mathbb{E}_t \mathbb{E}_{\mathbf{x}_\varepsilon} \mathbb{E}_{\mathbf{x}_t | \mathbf{x}_\varepsilon} [\|\mathbf{v}_t(\mathbf{x}_t; \theta) - \mathbf{u}_t(\mathbf{x}_t | \mathbf{x}_\varepsilon)\|^2], \quad (31)$$

where  $\mathbf{u}(\mathbf{x}_t | \mathbf{x}_\varepsilon)$  is the conditional probability path defined by the noising process and  $p(t) = U(\varepsilon, T)$ , is used to learn a vector field  $\mathbf{v}_t(\mathbf{x}_t; \theta)$  with parameters  $\theta$ . For this objective, and under the linear interpolation path where  $\alpha_t + \sigma_t = 1$ , Zhou et al. (2025) show that (29) is equivalent to,

$$\mathbf{s}(\mathbf{x}_t) = -\frac{\mathbf{x}_t + \alpha_t \mathbf{v}_t(\mathbf{x}_t)}{\sigma_t(\alpha_t + \sigma_t)}. \quad (32)$$

Plugging this into the baseline (10) gives us a new Stein baseline for this class of model:

$$b(\mathbf{x}_t) = -\left\langle \mathbf{v}_t(\mathbf{x}_t), -\frac{\mathbf{x}_t + \alpha_t \mathbf{v}_t(\mathbf{x}_t)}{\sigma_t(\alpha_t + \sigma_t)} \right\rangle. \quad (33)$$

Similarly, for the target residual  $r(\mathbf{x}_t)$ , we replace the score in (13) with (32) to obtain,

$$r(\mathbf{x}_t) = \langle \nabla, \mathbf{v}_t(\mathbf{x}_t) \rangle - \frac{\langle \mathbf{v}_t(\mathbf{x}_t), \mathbf{x}_t \rangle + \alpha_t \|\mathbf{v}_t(\mathbf{x}_t)\|^2}{\sigma_t(\alpha_t + \sigma_t)}. \quad (34)$$

After defining our baseline and residual, the rest of the *StAD* objective remains the same as for diffusion models (§3.1). Assuming our learned vector field is in Stein class, the Stein identity holds and gives us the same objective for  $\delta$ :

$$L(\delta; t) = \mathbb{E}_{\mathbf{x}_\varepsilon} \mathbb{E}_{\mathbf{x}_t | \mathbf{x}_\varepsilon} \left[ \delta^2(\mathbf{x}_t; t) + 2 \langle \nabla \delta(\mathbf{x}_t; t), \mathbf{v}_t(\mathbf{x}_t) \rangle \right], \quad (35)$$

We optimize our scalar head  $\delta(\mathbf{x}_t; t)$ , by minimizing the time average of  $L(\delta; t)$ , and approximate the target divergence by  $\langle \nabla, \mathbf{v}_t(\mathbf{x}_t) \rangle \approx b(\mathbf{x}_t) + \delta^*(\mathbf{x}_t; t)$ . A very similar approach can be taken for TrigFlow (Lu & Song, 2025)—a class of continuous-time consistency model—which we demonstrate in Appendix E.

### 3.3. Regularising $\delta$ to ensure validity of the StAD loss

We have derived *StAD* on the conditions that the models we are distilling are Gaussian bridges, and that the learned vector field is in Stein class. Appendix A examines the conditions under which  $\mathbf{v}_t(\mathbf{x}_t)$  will satisfy Stein boundary conditions (Liu et al., 2016; Liu & Wang, 2016; Gorham & Mackey, 2017; Gorham et al., 2019) for diffusion and flow-matching models.

In our derivation of the *StAD* loss, we have assumed that the boundary flux in (18) must vanish as  $R \rightarrow \infty$ . We can regularise  $\delta$  such that this occurs by construction. We define a regularised  $\hat{\delta}(\mathbf{x}) := \kappa_R(\mathbf{x})\delta(\mathbf{x})$ , with

$$\kappa_R = \begin{cases} 1; & \|\mathbf{x}\| \leq R \\ \frac{1}{2} + \frac{1}{2} \cos\left(\frac{\pi}{R}\|\mathbf{x}\| - \pi\right); & R < \|\mathbf{x}\| < 2R \\ 0; & \|\mathbf{x}\| \geq 2R \end{cases} \quad (36)$$

Between  $2R$  and  $R$ ,  $\kappa_R$  is a smooth transition between 1 and 0, using a cosine function. We set  $R$  such that  $\mathbb{P}_{\mathbf{x} \sim p}(\|\mathbf{x}\| > R)$  is negligible. This can be achieved by setting  $R$  to a high quantile of  $\|\mathbf{x}\|$ . This creates a compact support for  $\hat{\delta}$  and forces it to decay quickly. The only caveat here, is that if some probability mass lives outside of  $2R$ , it will be neglected. Now, that  $\hat{\delta}(\mathbf{x})$  has compact support, the boundary-flux term in (18),  $p(\mathbf{x})\delta(\mathbf{x})\mathbf{v}(\mathbf{x})$  vanishes regardless of the properties of  $\mathbf{v}(\mathbf{x})$  or  $p(\mathbf{x})$ . We can define the ball  $B$  on  $2R$ , and apply the divergence theorem as in (18), seeing that the boundary flux vanishes because,  $p(\mathbf{x})\hat{\delta}(\mathbf{x})\mathbf{v}(\mathbf{x}) = 0 \quad \forall \|\mathbf{x}\| \geq 2R$ .

Since,  $\hat{\delta}(\mathbf{x}) = \kappa_R\delta(\mathbf{x})$ , its derivative with respect to  $\mathbf{x}$  is

$$\nabla \hat{\delta}(\mathbf{x}) = \kappa_R(\mathbf{x})\nabla \delta(\mathbf{x}) + \delta(\mathbf{x})\nabla \kappa_R(\mathbf{x}). \quad (37)$$

This gives us a new regularised *StAD* objective:

$$L(\delta) = \mathbb{E}_{\mathbf{x}} \left[ \kappa_R^2(\mathbf{x})\delta^2(\mathbf{x}) + 2\kappa_R(\mathbf{x})\langle \nabla \delta(\mathbf{x}), \mathbf{v}(\mathbf{x}) \rangle + 2\delta(\mathbf{x})\langle \nabla \kappa_R(\mathbf{x}), \mathbf{v}(\mathbf{x}) \rangle \right]. \quad (38)$$

Since we define the transition in (36) to be cosine,  $\nabla \kappa_R$  when  $R < \|\mathbf{x}\| < 2R$  can be computed as,

$$\nabla \kappa_R(\mathbf{x}) = -\frac{\pi}{2R} \frac{\mathbf{x}}{\|\mathbf{x}\|} \sin\left(\frac{\pi}{R}\|\mathbf{x}\| - \pi\right), \quad (39)$$

and is zero otherwise.

In practice we include a further  $L^2$  penalty in the loss by adding  $\mathbb{E}_{\mathbf{x}}[l\|\nabla \hat{\delta}(\mathbf{x})\|^2]$  to (38). Here  $l$  can be set to regularise the gradient of  $\hat{\delta}(\mathbf{x})$  and ensure smoothness. We find in our experiments in §4 that the regularised objective gives more consistent outcomes, since the boundary condition assumed in (18) holds by construction.

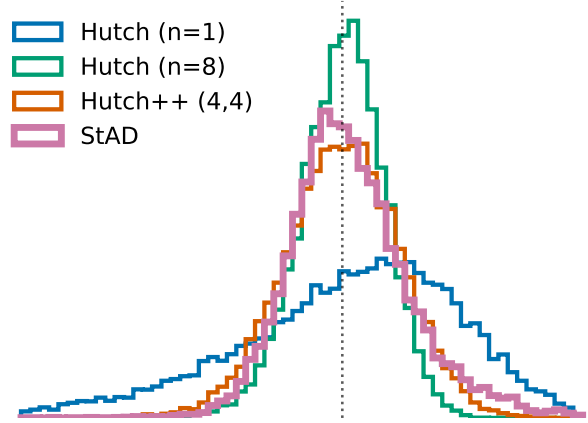


Figure 2. Divergence estimation for a VP-SDE diffusion model, trained to predict astrophysical fluxes and flux errors (26 dimensional conditional density). Histograms show log likelihood residuals (i.e. exact – estimated log likelihood) for Hutchinson with 1 and 8 probes, rank-4 Hutch++ with 4 probes, and *StAD*. Dotted line corresponds to zero residual.

## 4. Experiments and results

We test *StAD* on a variety of density estimation tasks using diffusion models, to evaluate its efficacy on low- to high-dimensional problems. We report the variance, mean-absolute error, and wall time for log-likelihood estimation compared to the exact trace, Hutchinson, Hutch++, and XTrace algorithms when predicting astrophysical fluxes and flux errors for the Cosmic Evolution Survey (COSMOS2020; Scoville et al., 2007; Weaver et al., 2022) in §4.1. In §4.2, we report negative log-likelihood (NLL) estimates along with variance and relative speedups on the CIFAR-10 (Krizhevsky, 2009) and ImageNet-32x32 (Chrabaszcz et al., 2017) datasets to show the scalability of our method. Full practical details of the experiments are given in Appendix F

### 4.1. Astrophysical fluxes

Simulation based inference and forward modelling for astronomical surveys relies on having a realistic generative model for the uncertainties on flux measurements (see e.g. Alsing et al., 2023; 2024; Crenshaw et al., 2024; Thorp et al., 2025), which is typically learned from data. As a test of *StAD*, we train a model for flux uncertainty conditional on magnitude (logarithmically scaled flux) using the COSMOS2020 dataset (Weaver et al., 2022). This is a  $26 \times 26$  conditional density estimation problem, with the model learning the distribution of 26 flux uncertainties conditional on 26 magnitudes (coming from 26 wavelength filters used in the COSMOS survey). The training data comprises  $\sim 420,000$  galaxies from COSMOS2020.

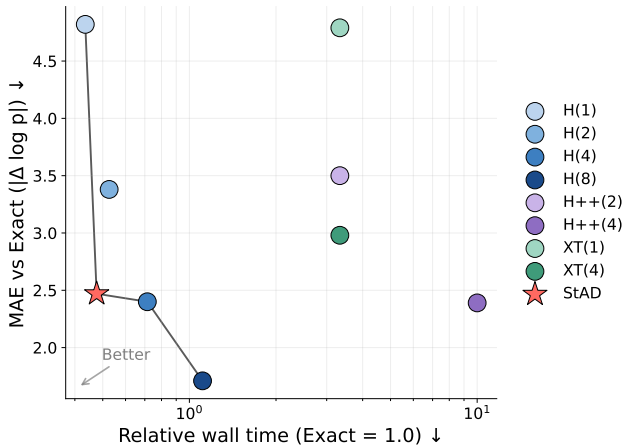


Figure 3. Pareto optimal divergence estimation with PF-ODEs. These are estimates for a VPSDE diffusion model predicting a 26 dimensional conditional density over astrophysical fluxes and flux errors. The figures plotted here are the same as in Table 1.

We train a variance preserving-SDE (VP-SDE) diffusion model that learns the conditional density (Thorpe et al., 2025); and distill it with *StAD*. The original *teacher* VP-SDE is trained via denoising score matching, and uses a  $256 \times 5$  multi-layered perceptron (MLP) as the score model. We use a  $512 \times 3$  MLP to distill the PF-ODE and learn a divergence estimator. We use the distilled model to estimate conditional probabilities for a set of test samples from COSMOS2020. We apply the Hutchinson, Hutch++, and XTrace estimators with different numbers of probes to the original VP-SDE, and compare all estimators to the exact trace, with results shown in Table 1, Figure 2, and Figure 3.

We find that *StAD* outperforms the stochastic estimators consistently in wall-time, with the exception of single-probe Hutchinson. *StAD* shows remarkably low mean-absolute-error (MAE) relative to the exact log likelihoods, as shown in Table 1. The only estimators that have a lower MAE and variance, are not much faster than the exact trace: Hutchinson with 4 or 8 probes and rank-4 Hutch++ or XTrace with 4 probes. The mean and standard deviation reports in Table 1 show that *StAD* is slightly biased compared to other trace estimators.

For Hutch++, we implement the FFJORD++ algorithm as shown in Liu et al. (2025), where we cache the  $Q$  matrix for the  $QR$  decomposition and refresh it every 6 iterations. However, we still find that computing  $QR$  decomposition dominates the cost and thus we find the Hutch++ to be even relatively slow in our tests. We plot the distribution of residuals for a subset of the estimators in Figure 2, noticing that the *StAD* residuals have a slight tail towards overestimates of the log likelihood (but less skew and variance than the Hutchinson estimator). The size of the distillation network

Table 1. Comparing the Hutchinson, Hutch++ and *StAD* log-likelihood estimates, to the exact trace for a diffusion model that predicts astrophysical flux uncertainties (§4.1). Methods:  $H(n)$  = Hutchinson with  $n$  probes;  $H++(n)$  = rank- $n$  Hutch++ with  $n$  probes;  $XT(n)$  = rank- $n$  XTrace with  $n$  probes; *StAD* = this work. Mean, standard deviation, MAE, and speedup are all measured relative to exact trace. NFEs are measured relative to the exact trace:  $rNFEs = NFEs [approx] / NFEs [exact]$ .

method	mean $\pm$ std	speedup ( $\times$ )	MAE	rNFEs
H(1)	0.06 $\pm$ 6.12	2.3	4.82	0.85
H(2)	0.03 $\pm$ 4.37	1.9	3.38	0.83
H(4)	0.00 $\pm$ 3.08	1.4	2.40	0.82
H(8)	0.00 $\pm$ 2.14	0.9	1.71	0.83
H++(2)	-0.08 $\pm$ 4.46	0.3	3.50	0.82
H++(4)	0.02 $\pm$ 2.98	0.1	2.39	0.82
XT(1)	-0.00 $\pm$ 6.15	0.3	4.79	0.82
XT(4)	-0.00 $\pm$ 3.74	0.3	2.98	0.82
<i>StAD</i>	0.46 $\pm$ 3.41	2.1	2.47	1.00

relative to the teacher directly affects the inference time for *StAD*; since the teacher network here was relatively compact, the relative speedups are modest. However, even though *StAD* has the same number of NFEs as the exact trace (seen in Table 1), it is still faster since we do not compute the Jacobian or its trace.

## 4.2. CIFAR-10 and ImageNet-32 $\times$ 32

We train a diffusion model with VP-SDE and U-Net architecture (Ronneberger et al., 2015) on CIFAR-10 and ImageNet-32 $\times$ 32. To distill these models, we use a compact convolutional neural network (CNN; LeCun et al., 1989a;b) with a linear time-embedding and Feature-wise Linear Modulation (FiLM; Perez et al., 2018) conditioning mechanism to inject time information into the spatial layers. We describe the architecture in more detail in Appendix F.

We compute negative log-likelihood (NLL) estimates from these models under matched ODE solver settings, expressing the results for each image in bits per dimension,

$$bpd(\mathbf{x}_\varepsilon) = \frac{-\log p(\mathbf{x}_\varepsilon)}{D \log 2} + \text{offset}. \quad (40)$$

Here we have an offset of 7, since the images are treated as continuous in  $[-1, 1]$  in the ODE, but in reality have an 8-bit discrete structure (Theis et al., 2016). Hence we report continuous NLL in *bpd* with the discretization offset, and add uniform dequantisation noise to the images. We evaluate NLLs using *StAD* and Hutchinson for a test set of 2048 images, computing the mean and standard deviation of NLL estimates across the sample. The results are summarized in Table 2 and Table 3.

We show that *StAD* remains competitive with the Hutchinson trace estimator, with consistent estimation of the mean NLL, whilst significantly reducing compute-time and com-

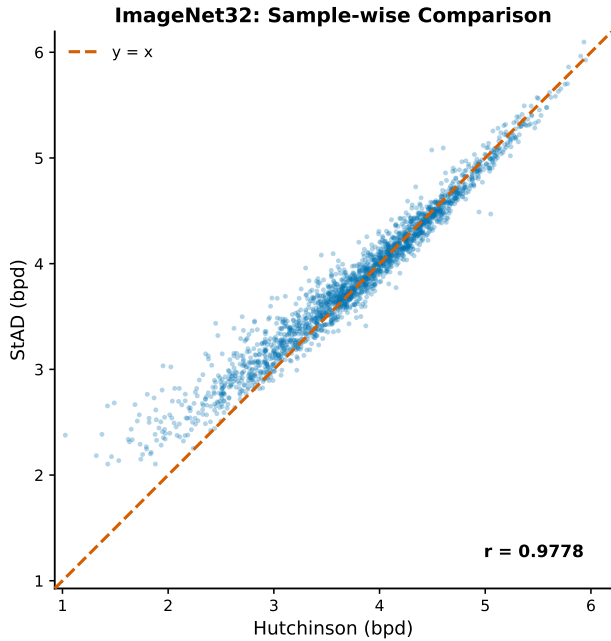


Figure 4. Sample-wise correlation test for NLL estimates from *StAD* vs. 2-probe Hutchinson, for 2048 images taken from ImageNet-32x32. Each blue point corresponds to one image.

plexity. For CIFAR-10, we observe that the difference in the mean NLL estimates is  $\sim 0.02$  bpd. Similarly, for ImageNet-32x32, we observe a difference in the mean NLL of  $\sim 0.07$  bpd. The NLL estimates from *StAD* show less variance when averaged across the test set. Additionally, in Figure 4 we perform a correlation test on a set of 2048 images, to compare the NLL estimates from Hutchinson with 2 probes against *StAD* on an image-by-image basis. We find for ImageNet-32x32 that the correlation coefficient is as high as  $\sim 0.98$ .

As seen in Figure 5, for CIFAR-10 the difference in NLL estimates between the two methods is generally small, albeit with some image-to-image scatter. We compute the amount of times the ODE drift term is evaluated (giving the number of NFEs) when integrating the likelihood; Table 2 and Table 3 show that *StAD* has a factor of  $\sim 4\times$  fewer NFEs than the single-probe Hutchinson estimator. Moreover, bypassing the Jacobian vector product required by Hutchinson leads to an additional speedup of  $\sim 2\times$  on top of the  $\sim 4\times$  reduction in NFEs. Further results for these datasets are included in Appendix G and H.

## 5. Discussion and conclusion

We present the *Stein Amortized Divergence* or *StAD* as a distillation technique to achieve pareto-optimal likelihood evaluations (Figure 3) for continuous time flows. We show that

Table 2. Comparing the Hutchinson and *StAD* NLL estimates for a VP-SDE diffusion model trained on CIFAR-10. NLLs are the mean and standard deviation across a test set of 2048 images. Speedup is measured relative to single-probe Hutchinson—H(1). NFEs are averaged over the total number per batch of 512 images.

method	NLL (bpd)	speedup ( $\times$ )	NFEs
H(1)	$3.403 \pm 0.583$	1.00	980
H(2)	$3.402 \pm 0.580$	0.65	970
<i>StAD</i>	$3.428 \pm 0.44$	7.24	250

Table 3. Comparing the Hutchinson and *StAD* NLL estimates for a diffusion model trained on ImageNet-32x32. Column definitions are as in Table 2.

method	NLL (bpd)	speedup ( $\times$ )	NFEs
H(1)	$3.783 \pm 0.787$	1.00	990
H(2)	$3.782 \pm 0.786$	0.65	981
<i>StAD</i>	$3.856 \pm 0.673$	7.56	240

our method can be generalised to a range of different generative paradigms (§3 and Appendix E), and demonstrate the efficacy of our method on diffusion workflows. *StAD* is a deterministic estimator of the divergence of the learned vector field, and thus provides smoother ODE trajectories, yielding faster likelihoods in addition to not requiring the Jacobian or its trace during inference. This is in contrast to scalable but stochastic estimators like the Hutchinson, Hutch++, and XTrace that still require Jacobian-vector products.

In workflows where frequent evaluations of the likelihood are needed, *StAD* is a promising alternative to traditional trace estimators. *StAD* is however not favourable when rare or sparse evaluations of the likelihood are needed, since it needs additional compute to distill the model in the first place. We find that the speedups achieved using *StAD* (compared to a stochastic estimator) are relative to the discrepancy between the student and teacher networks—a single JVP using the teacher network is of similar computational complexity to the forward pass through the student, assuming the architectural complexity is similar. If the student network is considerably more compact than the teacher, the potential gains from *StAD* distillation are much larger. This is seen in the discrepancy in speedups between Table 1 and Table 2 or Table 3 along with the difference in NFEs.

Future applications and tests of *StAD* are in: applying it to Boltzmann Generators (Noé et al., 2019; Rehman et al., 2026), where rapid and accurate likelihoods are necessary for importance weighting; aiding other distillation procedures and constructing flow-maps such as in Ai et al. (2026); improving flow and diffusion based modelling (Huang et al., 2025); guidance of diffusion models (Karczewski et al., 2025); black-box Bayesian optimisation as show in Yun et al. (2025); and out-of-distribution detection frameworks as shown in Raonic et al. (2026), to name a few.

## Likelihood Comparison: CIFAR-10

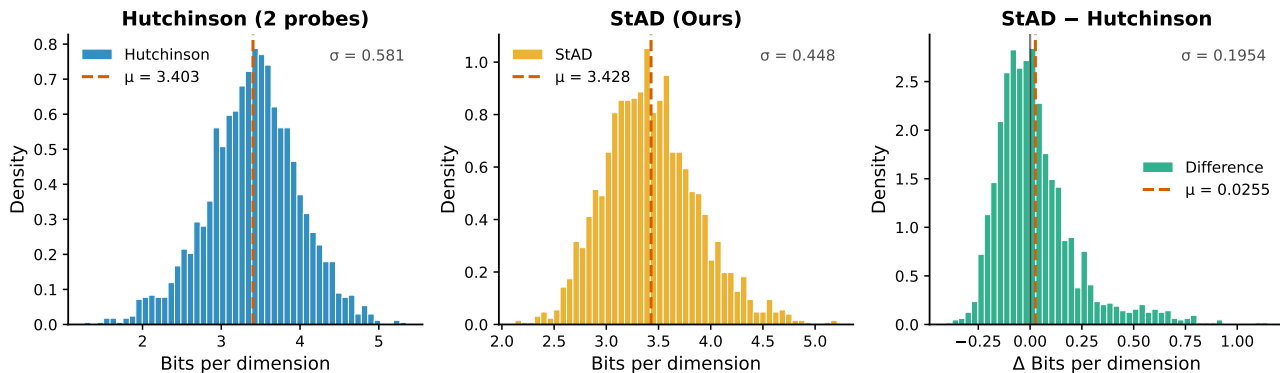


Figure 5. Sample-wise NLL estimates for CIFAR-10. *Left*: Using the Hutchinson algorithm with 2 probes. *Centre*: Using *StAD*. *Right*: Image-by-image difference between *StAD* and Hutchinson with 2 probes:  $\text{NLL}[\text{StAD}] - \text{NLL}[\text{H}(2)]$ .

## Acknowledgements

We thank Anik Halder and Justin Alsing for useful comments regarding the project and some of the source code. This work has been supported by funding from the European Research Council (ERC) under the European Union’s Horizon 2020 research and innovation programmes (grant agreement no. 101018897 CosmicExplorer and no. 818085 GMGalaxies), and the research project grant “Understanding the Dynamic Universe” funded by the Knut and Alice Wallenberg Foundation under Dnr KAW 2018.0067. This research utilized the Sunrise HPC facility supported by the Technical Division at the Department of Physics, Stockholm University.

## Impact Statement

This paper presents work whose goal is to advance the field of Machine Learning. There are many potential societal consequences of our work, none of which we feel must be specifically highlighted here.

## LLM Usage

We used LLMs to assist with code generation, verification, and as an initial research aid. The authors take full responsibility for the materials provided with this body of work.

## References

Adams, R. P., Pennington, J., Johnson, M. J., Smith, J., Ovadia, Y., Patton, B., and Saunderson, J. Estimating the spectral density of large implicit matrices. *preprint*, February 2018. URL <https://arxiv.org/abs/1802.03451>.

Ai, X., He, Y., Gu, A., Salakhutdinov, R., Zico Kolter, J., Boffi, N. M., and Simchowitz, M. Joint distillation for fast likelihood evaluation and sampling in flow-based models. In Vondrick, C. (ed.), *14th International Conference on Learning Representations*, April 2026. URL <https://openreview.net/forum?id=8uZ5UdIu12>.

Albergo, M., Boffi, N. M., and Vanden-Eijnden, E. Stochastic interpolants: A unifying framework for flows and diffusions. *Journal of Machine Learning Research*, 26(209):1–80, 2025. URL <http://jmlr.org/papers/v26/23-1605.html>.

Alsing, J., Charnock, T., Feeney, S., and Wandelt, B. Fast likelihood-free cosmology with neural density estimators and active learning. *Monthly Notices of the Royal Astronomical Society*, 488(3):4440–4458, September 2019. URL <https://doi.org/10.1093/mnras/stz1960>.

Alsing, J., Peiris, H., Mortlock, D., Leja, J., and Leistedt, B. Forward modeling of galaxy populations for cosmological redshift distribution inference. *The Astrophysical Journal Supplement Series*, 264(2):29, February 2023. URL <https://doi.org/10.3847/1538-4365/ac9583>.

Alsing, J., Thorp, S., Deger, S., Peiris, H. V., Leistedt, B., Mortlock, D., and Leja, J. pop-cosmos: A comprehensive picture of the galaxy population from COSMOS data. *The Astrophysical Journal Supplement Series*, 274(1):12, September 2024. URL <https://doi.org/10.3847/1538-4365/ad5c69>.

Anastasiou, A., Barp, A., Briol, F.-X., Ebner, B., Gaunt, R. E., Ghaderinezhad, F., Gorham, J., Gretton, A., Ley, C., Liu, Q., Mackey, L., Oates, C. J., Reinert, G., and

- Swan, Y. Stein’s method meets computational statistics: A review of some recent developments. *Statistical Science*, 38(1):120–139, 2023. URL <https://doi.org/10.1214/22-STS863>.
- Arnaudon, A., Holm, D. D., Pai, A., and Sommer, S. A stochastic large deformation model for computational anatomy. In Niethammer, M., Styner, M., Aylward, S., Zhu, H., Oguz, I., Yap, P.-T., and Shen, D. (eds.), *International Conference on Information Processing in Medical Imaging*, volume 10265 of *Lecture Notes in Computer Science*, pp. 571–582. Springer, 2017. URL [https://doi.org/10.1007/978-3-319-59050-9\\_45](https://doi.org/10.1007/978-3-319-59050-9_45).
- Arruda, J., Bracher, N., Köthe, U., Hasenauer, J., and Radev, S. T. Diffusion models in simulation-based inference: A tutorial review. *preprint*, December 2025. URL <https://arxiv.org/abs/2512.20685>.
- Avron, H. and Toledo, S. Randomized algorithms for estimating the trace of an implicit symmetric positive semi-definite matrix. *Journal of the Association for Computing Machinery*, 58(2):8, April 2011. URL <https://doi.org/10.1145/1944345.1944349>.
- Barbour, A. D. Stein’s method and poisson process convergence. *Journal of Applied Probability*, 25 (A):175–184, 1988. URL <https://doi.org/10.2307/3214155>.
- Barp, A., Briol, F.-X., Duncan, A. B., Girolami, M. A., and Mackey, L. W. Minimum Stein discrepancy estimators. In Wallach, H. M., Larochelle, H., Beygelzimer, A., d’Alché-Buc, F., Fox, E. B., and Garnett, R. (eds.), *Advances in Neural Information Processing Systems*, volume 32, pp. 12964–12976. Curran Associates, Inc., 2019. URL [https://proceedings.neurips.cc/paper\\_files/paper/2019/file/ba7609ee5789cc4dff171045a693a65f-Paper.pdf](https://proceedings.neurips.cc/paper_files/paper/2019/file/ba7609ee5789cc4dff171045a693a65f-Paper.pdf).
- Bénard, C., Staber, B., and Da Veiga, S. Kernel Stein discrepancy thinning: a theoretical perspective of pathologies and a practical fix with regularization. In Oh, A., Naumann, T., Globerson, A., Saenko, K., Hardt, M., and Levine, S. (eds.), *Advances in Neural Information Processing Systems*, volume 36, pp. 49281–49311. Curran Associates, Inc., 2023. URL [https://proceedings.neurips.cc/paper\\_files/paper/2023/file/9a8eb202c060b7d81f5889631cbcd47e-Paper-Conference.pdf](https://proceedings.neurips.cc/paper_files/paper/2023/file/9a8eb202c060b7d81f5889631cbcd47e-Paper-Conference.pdf).
- Biloš, M. and Günnemann, S. Scalable normalizing flows for permutation invariant densities. In Meila, M. and Zhang, T. (eds.), *Proceedings of the 38th International Conference on Machine Learning*, volume 139 of *Proceedings of Machine Learning Research*, pp. 957–967. PMLR, July 2021. URL <https://proceedings.mlr.press/v139/bilos21a.html>.
- Chen, R. T. Q. and Duvenaud, D. K. Neural networks with cheap differential operators. In Wallach, H., Larochelle, H., Beygelzimer, A., d’Alché-Buc, F., Fox, E., and Garnett, R. (eds.), *Advances in Neural Information Processing Systems*, volume 32, pp. 9961–9971. Curran Associates, Inc., 2019. URL [https://proceedings.neurips.cc/paper\\_files/paper/2019/file/770f8e448d07586afbf77bb59f698587-Paper.pdf](https://proceedings.neurips.cc/paper_files/paper/2019/file/770f8e448d07586afbf77bb59f698587-Paper.pdf).
- Chen, R. T. Q., Rubanova, Y., Bettencourt, J., and Duvenaud, D. K. Neural ordinary differential equations. In Bengio, S., Wallach, H., Larochelle, H., Grauman, K., Cesa-Bianchi, N., and Garnett, R. (eds.), *Advances in Neural Information Processing Systems*, volume 31, pp. 6572–6583. Curran Associates, Inc., 2018a. URL [https://proceedings.neurips.cc/paper\\_files/paper/2018/file/69386f6bb1dfed68692a24c8686939b9-Paper.pdf](https://proceedings.neurips.cc/paper_files/paper/2018/file/69386f6bb1dfed68692a24c8686939b9-Paper.pdf).
- Chen, W. Y., Mackey, L., Gorham, J., Briol, F.-X., and Oates, C. Stein points. In Dy, J. and Krause, A. (eds.), *Proceedings of the 35th International Conference on Machine Learning*, volume 80 of *Proceedings of Machine Learning Research*, pp. 844–853. PMLR, July 2018b. URL <https://proceedings.mlr.press/v80/chen18f.html>.
- Chrabaszcz, P., Loshchilov, I., and Hutter, F. A down-sampled variant of ImageNet as an alternative to the CIFAR datasets. *preprint*, July 2017. URL <https://arxiv.org/abs/1707.08819>.
- Chwialkowski, K., Strathmann, H., and Gretton, A. A kernel test of goodness of fit. In Balcan, M. F. and Weinberger, K. Q. (eds.), *Proceedings of The 33rd International Conference on Machine Learning*, volume 48 of *Proceedings of Machine Learning Research*, pp. 2606–2615. PMLR, June 2016. URL <https://proceedings.mlr.press/v48/chwialkowski16.html>.
- Crenshaw, J. F., Kalmbach, J. B., Gagliano, A., Yan, Z., Connolly, A. J., Malz, A. I., Schmidt, S. J., and The LSST Dark Energy Science Collaboration. Probabilistic forward modeling of galaxy catalogs with normalizing flows. *The Astronomical Journal*, 168(2):80, August 2024. URL <https://doi.org/10.3847/1538-3881/ad54bf>.

- Dinh, L., Krueger, D., and Bengio, Y. NICE: non-linear independent components estimation. In Bengio, Y. and LeCun, Y. (eds.), *3rd International Conference on Learning Representations*, May 2015. URL <http://arxiv.org/abs/1410.8516>.
- Dormand, J. and Prince, P. A family of embedded Runge–Kutta formulae. *Journal of Computational and Applied Mathematics*, 6(1):19–26, 1980. URL [https://doi.org/10.1016/0771-050X\(80\)90013-3](https://doi.org/10.1016/0771-050X(80)90013-3).
- Efron, B. Tweedie’s formula and selection bias. *Journal of the American Statistical Association*, 106(496):1602–1614, 2011. URL <https://doi.org/10.1198/jasa.2011.tm11181>.
- Epperly, E. N., Tropp, J. A., and Webber, R. J. XTRACE: Making the most of every sample in stochastic trace estimation. *SIAM Journal on Matrix Analysis and Applications*, 45(1):1–23, January 2024. URL <https://doi.org/10.1137/23M1548323>.
- Gambhir, A. S., Stathopoulos, A., and Orginos, K. Deflation as a method of variance reduction for estimating the trace of a matrix inverse. *SIAM Journal on Scientific Computing*, 39(2):A532–A558, 2017. URL <https://doi.org/10.1137/16M1066361>.
- Geng, Z., Deng, M., Bai, X., Kolter, Z., and He, K. Mean flows for one-step generative modeling. In Belgrave, D., Zhang, C., Lin, H., Pascanu, R., Koniusz, P., Ghassemi, M., and Chen, N. (eds.), *Advances in Neural Information Processing Systems*, volume 38, pp. 75460–75482. Curran Associates, Inc., 2025. URL [https://proceedings.neurips.cc/paper\\_files/paper/2025/file/6d13e085b79d454da5910e4ca82a3d9d-Paper-Conference.pdf](https://proceedings.neurips.cc/paper_files/paper/2025/file/6d13e085b79d454da5910e4ca82a3d9d-Paper-Conference.pdf).
- Girard, D. A. A fast ‘Monte-Carlo cross-validation’ procedure for large least squares problems with noisy data. *Numerische Mathematik*, 56:1–23, 1989. URL <https://doi.org/10.1007/BF01395775>.
- Gittens, A. and Mahoney, M. Revisiting the Nyström method for improved large-scale machine learning. In Dasgupta, S. and McAllester, D. (eds.), *Proceedings of the 30th International Conference on Machine Learning*, volume 28 of *Proceedings of Machine Learning Research*, pp. 567–575. PMLR, June 2013. URL <https://proceedings.mlr.press/v28/gittens13.html>.
- Gorham, J. and Mackey, L. Measuring sample quality with kernels. In Precup, D. and Teh, Y. W. (eds.), *Proceedings of the 34th International Conference on Machine Learning*, volume 70 of *Proceedings of Machine Learning Research*, pp. 1292–1301. PMLR, August 2017. URL <https://proceedings.mlr.press/v70/gorham17a.html>.
- Gorham, J. and Mackey, L. W. Measuring sample quality with Stein’s method. In Cortes, C., Lawrence, N. D., Lee, D. D., Sugiyama, M., and Garnett, R. (eds.), *Advances in Neural Information Processing Systems*, volume 28, pp. 226–234. Curran Associates, Inc., 2015. URL [https://papers.nips.cc/paper\\_files/paper/2015/file/698d51a19d8a121ce581499d7b701668-Paper.pdf](https://papers.nips.cc/paper_files/paper/2015/file/698d51a19d8a121ce581499d7b701668-Paper.pdf).
- Gorham, J., Duncan, A. B., Vollmer, S. J., and Mackey, L. Measuring sample quality with diffusions. *The Annals of Applied Probability*, 29(5):2884–2928, 2019. URL <https://doi.org/10.1214/19-AAP1467>.
- Grathwohl, W., Chen, R. T. Q., Bettencourt, J., Sutskever, I., and Duvenaud, D. FFJORD: Free-form continuous dynamics for scalable reversible generative models. In Sainath, T. (ed.), *7th International Conference on Learning Representations*, May 2019. URL <https://openreview.net/forum?id=rJxgknCcK7>.
- Grathwohl, W., Wang, K.-C., Jacobsen, J.-H., Duvenaud, D., and Zemel, R. Learning the Stein discrepancy for training and evaluating energy-based models without sampling. In Daumé, III, H. and Singh, A. (eds.), *Proceedings of the 37th International Conference on Machine Learning*, volume 119 of *Proceedings of Machine Learning Research*, pp. 3732–3747. PMLR, July 2020. URL <https://proceedings.mlr.press/v119/grathwohl20a.html>.
- Ho, J., Jain, A., and Abbeel, P. Denoising diffusion probabilistic models. In Larochelle, H., Ranzato, M., Hadsell, R., Balcan, M., and Lin, H. (eds.), *Advances in Neural Information Processing Systems*, volume 33, pp. 6840–6851. Curran Associates, Inc., 2020. URL [https://proceedings.neurips.cc/paper\\_files/paper/2020/file/4c5bcfec8584af0d967f1ab10179ca4b-Paper.pdf](https://proceedings.neurips.cc/paper_files/paper/2020/file/4c5bcfec8584af0d967f1ab10179ca4b-Paper.pdf).
- Huang, Y., Transue, T., Wang, S.-H., Feldman, W. M., Zhang, H., and Wang, B. Improving flow matching by aligning flow divergence. In Singh, A., Fazel, M., Hsu, D., Lacoste-Julien, S., Berkenkamp, F., Maharaj, T., Wagstaff, K., and Zhu, J. (eds.), *Proceedings of the 42nd International Conference on Machine Learning*, volume 267 of *Proceedings of Machine Learning Research*, pp. 25813–25834. PMLR, July 2025. URL <https://proceedings.mlr.press/v267/huang25ag.html>.

- Hutchinson, M. F. A stochastic estimator of the trace of the influence matrix for Laplacian smoothing splines. *Communications in Statistics – Simulation and Computation*, 18(3):1059–1076, 1989. URL <https://doi.org/10.1080/03610918908812806>.
- Hyvärinen, A. Estimation of non-normalized statistical models by score matching. *Journal of Machine Learning Research*, 6(24):695–709, 2005. URL <http://jmlr.org/papers/v6/hyvarinen05a.html>.
- Jiang, S., Pham, H., Woodruff, D., and Zhang, R. Optimal sketching for trace estimation. In Ranzato, M., Beygelzimer, A., Dauphin, Y., Liang, P. S., and Vaughan, J. W. (eds.), *Advances in Neural Information Processing Systems*, volume 34, pp. 23741–23753. Curran Associates, Inc., 2021. URL [https://proceedings.neurips.cc/paper\\_files/paper/2021/file/c77bfda61a0204d445185053e6a9a8fe-Paper.pdf](https://proceedings.neurips.cc/paper_files/paper/2021/file/c77bfda61a0204d445185053e6a9a8fe-Paper.pdf).
- Karczewski, R., Heinonen, M., and Garg, V. Diffusion models as cartoonists: The curious case of high density regions. In Yue, Y. (ed.), *13th International Conference on Learning Representations*, April 2025. URL <https://openreview.net/forum?id=RiS2cxpENN>.
- Karras, T., Aittala, M., Aila, T., and Laine, S. Elucidating the design space of diffusion-based generative models. In Koyejo, S., Mohamed, S., Agarwal, A., Belgrave, D., Cho, K., and Oh, A. (eds.), *Advances in Neural Information Processing Systems*, volume 35, pp. 26565–26577. Curran Associates, Inc., 2022. URL [https://proceedings.neurips.cc/paper\\_files/paper/2022/file/a98846e9d9cc01cfb87eb694d946ce6b-Paper-Conference.pdf](https://proceedings.neurips.cc/paper_files/paper/2022/file/a98846e9d9cc01cfb87eb694d946ce6b-Paper-Conference.pdf).
- Karras, T., Aittala, M., Lehtinen, J., Hellsten, J., Aila, T., and Laine, S. Analyzing and improving the training dynamics of diffusion models. In *2024 IEEE/CVF Conference on Computer Vision and Pattern Recognition (CVPR)*, pp. 24174–24184, Los Alamitos, CA, USA, June 2024. IEEE Computer Society. URL <https://doi.org/10.1109/CVPR52733.2024.02282>.
- Kingma, D. and Gao, R. Understanding diffusion objectives as the ELBO with simple data augmentation. In Oh, A., Naumann, T., Globerson, A., Saenko, K., Hardt, M., and Levine, S. (eds.), *Advances in Neural Information Processing Systems*, volume 36, pp. 65484–65516. Curran Associates, Inc., 2023. URL [https://proceedings.neurips.cc/paper\\_files/paper/2023/file/ce79fbf9baef726645bc2337abb0ade2-Paper-Conference.pdf](https://proceedings.neurips.cc/paper_files/paper/2023/file/ce79fbf9baef726645bc2337abb0ade2-Paper-Conference.pdf).
- Kobyzev, I., Prince, S. J., and Brubaker, M. A. Normalizing flows: An introduction and review of current methods. *IEEE Transactions on Pattern Analysis and Machine Intelligence*, 43(11):3964–3979, 2021. URL <https://doi.org/10.1109/TPAMI.2020.2992934>.
- Krizhevsky, A. Learning multiple layers of features from tiny images. Technical report, Computer Science, University of Toronto, April 2009. URL <https://www.cs.toronto.edu/~kriz/learning-features-2009-TR.pdf>.
- LeCun, Y., Boser, B., Denker, J., Henderson, D., Howard, R., Hubbard, W., and Jackel, L. Handwritten digit recognition with a back-propagation network. In Touretzky, D. (ed.), *Advances in Neural Information Processing Systems*, volume 2, pp. 396–404. Morgan-Kaufmann, 1989a. URL [https://proceedings.neurips.cc/paper\\_files/paper/1989/file/53c3bce66e43be4f209556518c2fcb54-Paper.pdf](https://proceedings.neurips.cc/paper_files/paper/1989/file/53c3bce66e43be4f209556518c2fcb54-Paper.pdf).
- LeCun, Y., Boser, B., Denker, J. S., Henderson, D., Howard, R. E., Hubbard, W., and Jackel, L. D. Backpropagation applied to handwritten zip code recognition. *Neural Computation*, 1(4):541–551, 1989b. URL <https://doi.org/10.1162/neco.1989.1.4.541>.
- Li, H. and Zhu, Y. Randomized block Krylov subspace methods for trace and log-determinant estimators. *BIT Numerical Mathematics*, 61:911–939, September 2021. URL <https://doi.org/10.1007/s10543-021-00850-7>.
- Lin, L. Randomized estimation of spectral densities of large matrices made accurate. *Numerische Mathematik*, 136:183–213, May 2017. URL <https://doi.org/10.1007/s00211-016-0837-7>.
- Lin, L., Saad, Y., and Yang, C. Approximating spectral densities of large matrices. *SIAM Review*, 58(1):34–65, 2016. URL <https://doi.org/10.1137/130934283>.
- Lipman, Y., Chen, R. T. Q., Ben-Hamu, H., Nickel, M., and Le, M. Flow matching for generative modeling. In Liu, Y. (ed.), *11th International Conference on Learning Representations*, May 2023. URL <https://openreview.net/forum?id=PqvMRDCJT9t>.
- Lipman, Y., Havasi, M., Holderrieth, P., Shaul, N., Le, M., Karrer, B., Chen, R. T. Q., Lopez-Paz, D., Ben-Hamu, H., and Gat, I. Flow matching guide and code. *preprint*, December 2024. URL <https://arxiv.org/abs/2412.06264>.
- Liu, Q. and Wang, D. Stein variational gradient descent: A general purpose Bayesian inference algorithm. In Lee, D.,

- Sugiyama, M., Luxburg, U., Guyon, I., and Garnett, R. (eds.), *Advances in Neural Information Processing Systems*, volume 29, pp. 2378–2386. Curran Associates, Inc., 2016. URL [https://proceedings.neurips.cc/paper\\_files/paper/2016/file/b3ba8f1bee1238a2f37603d90b58898d-Paper.pdf](https://proceedings.neurips.cc/paper_files/paper/2016/file/b3ba8f1bee1238a2f37603d90b58898d-Paper.pdf).
- Liu, Q., Lee, J., and Jordan, M. A kernelized Stein discrepancy for goodness-of-fit tests. In Balcan, M. F. and Weinberger, K. Q. (eds.), *Proceedings of The 33rd International Conference on Machine Learning*, volume 48 of *Proceedings of Machine Learning Research*, pp. 276–284. PMLR, June 2016. URL <https://proceedings.mlr.press/v48/liub16.html>.
- Liu, X., Gong, C., and Liu, Q. Flow straight and fast: Learning to generate and transfer data with rectified flow. In Liu, Y. (ed.), *11th International Conference on Learning Representations*, May 2023. URL <https://openreview.net/forum?id=XVjTtlw5z>.
- Liu, X., Zhang, X., Ma, J., Peng, J., and Liu, Q. InstaFlow: One step is enough for high-quality diffusion-based text-to-image generation. In Kim, B. (ed.), *12th International Conference on Learning Representations*, May 2024. URL <https://openreview.net/forum?id=1k4yZbbDqX>.
- Liu, X., Du, H., Deng, W., and Zhang, R. Optimal stochastic trace estimation in generative modeling. In Li, Y., Mandt, S., Agrawal, S., and Khan, E. (eds.), *Proceedings of The 28th International Conference on Artificial Intelligence and Statistics*, volume 258 of *Proceedings of Machine Learning Research*, pp. 4600–4608. PMLR, May 2025. URL <https://proceedings.mlr.press/v258/liu25k.html>.
- Lu, C. and Song, Y. Simplifying, stabilizing and scaling continuous-time consistency models. In Yue, Y. (ed.), *13th International Conference on Learning Representations*, April 2025. URL <https://openreview.net/forum?id=LyJi5ugyJx>.
- Luhman, E. and Luhman, T. Knowledge distillation in iterative generative models for improved sampling speed. *preprint*, February 2021. URL <https://arxiv.org/abs/2101.02388>.
- Luo, W., Hu, T., Zhang, S., Sun, J., Li, Z., and Zhang, Z. Diff-Instruct: A universal approach for transferring knowledge from pre-trained diffusion models. In Oh, A., Naumann, T., Globerson, A., Saenko, K., Hardt, M., and Levine, S. (eds.), *Advances in Neural Information Processing Systems*, volume 36, pp. 76525–76546. Curran Associates, Inc., 2023. URL [https://proceedings.neurips.cc/paper\\_files/paper/2023/file/f115f619b62833aad5ac058975b0e6-Paper-Conference.pdf](https://proceedings.neurips.cc/paper_files/paper/2023/file/f115f619b62833aad5ac058975b0e6-Paper-Conference.pdf).
- Maoutsa, D., Reich, S., and Opper, M. Interacting particle solutions of Fokker–Planck equations through gradient-log-density estimation. *Entropy*, 22(8):802, July 2020. URL <https://doi.org/10.3390/e22080802>.
- Meyer, R. A., Musco, C., Musco, C., and Woodruff, D. P. Hutch++: Optimal stochastic trace estimation. In King, V. and Le, H. V. (eds.), *2021 Symposium on Simplicity in Algorithms (SOSA)*, pp. 142–155, 2021. URL <https://doi.org/10.1137/1.9781611976496.16>.
- Noé, F., Olsson, S., Köhler, J., and Wu, H. Boltzmann generators: Sampling equilibrium states of many-body systems with deep learning. *Science*, 365(6457):aaw1147, September 2019. URL <https://doi.org/10.1126/science.aaw1147>.
- Oates, C. J., Girolami, M., and Chopin, N. Control functionals for Monte Carlo integration. *Journal of the Royal Statistical Society Series B: Statistical Methodology*, 79(3):695–718, May 2016. URL <https://doi.org/10.1111/rssb.12185>.
- Papamakarios, G., Nalisnick, E., Rezende, D. J., Mohamed, S., and Lakshminarayanan, B. Normalizing flows for probabilistic modeling and inference. *Journal of Machine Learning Research*, 22(57):1–64, 2021. URL <http://jmlr.org/papers/v22/19-1028.html>.
- Paszke, A., Gross, S., Massa, F., Lerer, A., Bradbury, J., Chanan, G., Killeen, T., Lin, Z., Gimelshein, N., Antiga, L., Desmaison, A., Kopf, A., Yang, E., DeVito, Z., Raison, M., Tejani, A., Chilamkurthy, S., Steiner, B., Fang, L., Bai, J., and Chintala, S. PyTorch: An imperative style, high-performance deep learning library. In Wallach, H., Larochelle, H., Beygelzimer, A., d’Alché-Buc, F., Fox, E., and Garnett, R. (eds.), *Advances in Neural Information Processing Systems*, volume 32, pp. 8024–8035. Curran Associates, Inc., 2019. URL [https://proceedings.neurips.cc/paper\\_files/paper/2019/file/bdbca288fee7f92f2bfa9f7012727740-Paper.pdf](https://proceedings.neurips.cc/paper_files/paper/2019/file/bdbca288fee7f92f2bfa9f7012727740-Paper.pdf).
- Perez, E., Strub, F., de Vries, H., Dumoulin, V., and Courville, A. FiLM: visual reasoning with a general conditioning layer. In *Proceedings of the Thirty-Second AAAI Conference on Artificial Intelligence, AAAI’18/IAAI’18/EAAI’18*. AAAI Press, 2018. URL <https://doi.org/10.1609/aaai.v32i1.11671>.

- Persson, D., Cortinovis, A., and Kressner, D. Improved variants of the Hutch++ algorithm for trace estimation. *SIAM Journal on Matrix Analysis and Applications*, 43(3):1162–1185, 2022. URL <https://doi.org/10.1137/21M1447623>.
- Ranganath, R., Tran, D., Altsosaar, J., and Blei, D. Operator variational inference. In Lee, D., Sugiyama, M., Luxburg, U., Guyon, I., and Garnett, R. (eds.), *Advances in Neural Information Processing Systems*, volume 29, pp. 496–504. Curran Associates, Inc., 2016. URL [https://proceedings.neurips.cc/paper\\_files/paper/2016/file/d947bf06a885db0d477d707121934ff8-Paper.pdf](https://proceedings.neurips.cc/paper_files/paper/2016/file/d947bf06a885db0d477d707121934ff8-Paper.pdf).
- Raonic, B., Mishra, S., and Lanthaler, S. Towards a certificate of trust: Task-aware OOD detection for scientific AI. In Vondrick, C. (ed.), *14th International Conference on Learning Representations*, April 2026. URL <https://openreview.net/forum?id=2RuSWLQK82>.
- Rehman, D., Akhound-Sadegh, T., Gazizov, A., Bengio, Y., and Tong, A. FALCON: Few-step accurate likelihoods for continuous flows. In Vondrick, C. (ed.), *14th International Conference on Learning Representations*, April 2026. URL <https://openreview.net/forum?id=FbssShlI4N>.
- Riabiz, M., Chen, W. Y., Cockayne, J., Swietach, P., Niederer, S. A., Mackey, L., and Oates, C. J. Optimal thinning of MCMC output. *Journal of the Royal Statistical Society Series B: Statistical Methodology*, 84(4):1059–1081, April 2022. URL <https://doi.org/10.1111/rssb.12503>.
- Robbins, H. E. An empirical Bayes approach to statistics. In Kotz, S. and Johnson, N. L. (eds.), *Breakthroughs in Statistics: Foundations and Basic Theory*, Springer Series in Statistics, pp. 388–394. Springer, 1992. URL [https://doi.org/10.1007/978-1-4612-0919-5\\_26](https://doi.org/10.1007/978-1-4612-0919-5_26).
- Ronneberger, O., Fischer, P., and Brox, T. U-Net: Convolutional networks for biomedical image segmentation. In Navab, N., Hornegger, J., Wells, W. M., and Frangi, A. F. (eds.), *Medical Image Computing and Computer-Assisted Intervention – MICCAI 2015*, volume 9351 of *Lecture Notes in Computer Science*, pp. 234–241. Springer International Publishing, 2015. URL [https://doi.org/10.1007/978-3-319-24574-4\\_28](https://doi.org/10.1007/978-3-319-24574-4_28).
- Roosta-Khorasani, F. and Ascher, U. Improved bounds on sample size for implicit matrix trace estimators. *Foundations of Computational Mathematics*, 15:1187–1212, September 2015. URL <https://doi.org/10.1007/s10208-014-9220-1>.
- Sabour, A., Fidler, S., and Kreis, K. Align your flow: Scaling continuous-time flow map distillation. In Belgrave, D., Zhang, C., Lin, H., Pascanu, R., Koniusz, P., Ghassemi, M., and Chen, N. (eds.), *Advances in Neural Information Processing Systems*, volume 38, pp. 146459–146512. Curran Associates, Inc., 2025. URL [https://proceedings.neurips.cc/paper\\_files/paper/2025/file/d79ac139911df25d27f14bbf008deae-Paper-Conference.pdf](https://proceedings.neurips.cc/paper_files/paper/2025/file/d79ac139911df25d27f14bbf008deae-Paper-Conference.pdf).
- Saibaba, A. K., Alexanderian, A., and Ipsen, I. C. Randomized matrix-free trace and log-determinant estimators. *Numerische Mathematik*, 137:353–395, October 2017. URL <https://doi.org/10.1007/s00211-017-0880-z>.
- Salimans, T. and Ho, J. Progressive distillation for fast sampling of diffusion models. In Hofmann, K. and Rush, A. (eds.), *10th International Conference on Learning Representations*, April 2022. URL <https://openreview.net/forum?id=TIIdIXIpzhoI>.
- Sauer, A., Lorenz, D., Blattmann, A., and Rombach, R. Adversarial diffusion distillation. In Leonardis, A., Ricci, E., Roth, S., Russakovsky, O., Sattler, T., and Varol, G. (eds.), *Computer Vision – ECCV 2024*, volume 15144 of *Lecture Notes in Computer Science*, pp. 87–103. Springer Nature Switzerland, 2025. URL [https://doi.org/10.1007/978-3-031-73016-0\\_6](https://doi.org/10.1007/978-3-031-73016-0_6).
- Schebek, M., Noé, F., and Rogal, J. Scalable Boltzmann generators for equilibrium sampling of large-scale materials. *preprint*, September 2025. URL <https://arxiv.org/abs/2509.25486>.
- Scoville, N., Aussel, H., Brusa, M., Capak, P., Carollo, C. M., Elvis, M., Giavalisco, M., Guzzo, L., Hasinger, G., Impey, C., Kneib, J.-P., LeFevre, O., Lilly, S. J., Mobasher, B., Renzini, A., Rich, R. M., Sanders, D. B., Schinnerer, E., Schminovich, D., Shopbell, P., Taniguchi, Y., and Tyson, N. D. The Cosmic Evolution Survey (COSMOS): Overview. *The Astrophysical Journal Supplement Series*, 172(1):1–8, September 2007. URL <https://doi.org/10.1086/516585>.
- Silver, R. N. and Röder, H. Densities of states of mega-dimensional Hamiltonian matrices. *International Journal of Modern Physics C*, 5(4):735–753, January 1994. URL <https://doi.org/10.1142/S0129183194000842>.
- Skilling, J. The Eigenvalues of mega-dimensional matrices. In Skilling, J. (ed.), *Maximum Entropy and Bayesian Methods*, volume 36 of *Fundamental Theories of Physics*, pp. 455–466. Springer, 1989. URL [https://doi.org/10.1007/978-94-015-7860-8\\_48](https://doi.org/10.1007/978-94-015-7860-8_48).

- Sohl-Dickstein, J., Weiss, E., Maheswaranathan, N., and Ganguli, S. Deep unsupervised learning using nonequilibrium thermodynamics. In Bach, F. and Blei, D. (eds.), *Proceedings of the 32nd International Conference on Machine Learning*, volume 37 of *Proceedings of Machine Learning Research*, pp. 2256–2265. PMLR, July 2015. URL <https://proceedings.mlr.press/v37/sohl-dickstein15.html>.
- Song, Y. and Dhariwal, P. Improved techniques for training consistency models. In Kim, B. (ed.), *12th International Conference on Learning Representations*, May 2024. URL <https://openreview.net/forum?id=WNzy9bRDvG>.
- Song, Y. and Ermon, S. Generative modeling by estimating gradients of the data distribution. In Wallach, H. M., Larochelle, H., Beygelzimer, A., d’Alché-Buc, F., Fox, E. B., and Garnett, R. (eds.), *Advances in Neural Information Processing Systems*, volume 32, pp. 11895–11907. Curran Associates, Inc., 2019. URL [https://proceedings.neurips.cc/paper\\_files/paper/2019/file/3001ef257407d5a371a96dcd947c7d93-Paper.pdf](https://proceedings.neurips.cc/paper_files/paper/2019/file/3001ef257407d5a371a96dcd947c7d93-Paper.pdf).
- Song, Y. and Ermon, S. Improved techniques for training score-based generative models. In Larochelle, H., Ranzato, M., Hadsell, R., Balcan, M., and Lin, H. (eds.), *Advances in Neural Information Processing Systems*, volume 33, pp. 12438–12448. Curran Associates, Inc., 2020. URL [https://proceedings.neurips.cc/paper\\_files/paper/2020/file/92c3b916311a5517d9290576e3ea37ad-Paper.pdf](https://proceedings.neurips.cc/paper_files/paper/2020/file/92c3b916311a5517d9290576e3ea37ad-Paper.pdf).
- Song, Y., Durkan, C., Murray, I., and Ermon, S. Maximum likelihood training of score-based diffusion models. In Ranzato, M., Beygelzimer, A., Dauphin, Y., Liang, P., and Vaughan, J. W. (eds.), *Advances in Neural Information Processing Systems*, volume 34, pp. 1415–1428. Curran Associates, Inc., 2021a. URL [https://proceedings.neurips.cc/paper\\_files/paper/2021/file/0a9fdbb17feb6ccb7ec405cfb85222c4-Paper.pdf](https://proceedings.neurips.cc/paper_files/paper/2021/file/0a9fdbb17feb6ccb7ec405cfb85222c4-Paper.pdf).
- Song, Y., Sohl-Dickstein, J., Kingma, D. P., Kumar, A., Ermon, S., and Poole, B. Score-based generative modeling through stochastic differential equations. In Mohamed, S. (ed.), *9th International Conference on Learning Representations*, May 2021b. URL <https://openreview.net/forum?id=PxTIG12RRHS>.
- Song, Y., Dhariwal, P., Chen, M., and Sutskever, I. Consistency models. In Krause, A., Brunskill, E., Cho, K., Engelhardt, B., Sabato, S., and Scarlett, J. (eds.), *Proceedings of the 40th International Conference on Machine Learning*, volume 202 of *Proceedings of Machine Learning Research*, pp. 32211–32252. PMLR, July 2023. URL <https://proceedings.mlr.press/v202/song23a.html>.
- Stein, C. A bound for the error in the normal approximation to the distribution of a sum of dependent random variables. In Le Cam, L. M., Neyman, J., and Scott, E. L. (eds.), *Proceedings of the sixth Berkeley symposium on mathematical statistics and probability, volume 2: Probability theory*, volume 6.2 of *Berkeley Symposium on Mathematical Statistics*, pp. 583–603. University of California Press, 1972.
- Theis, L., van den Oord, A., and Bethge, M. A note on the evaluation of generative models. In Bengio, Y. and LeCun, Y. (eds.), *4th International Conference on Learning Representations*, May 2016. URL <http://arxiv.org/abs/1511.01844>.
- Thorp, S., Peiris, H. V., Jagwani, G., Deger, S., Alsing, J., Leistedt, B., Mortlock, D. J., Halder, A., and Leja, J. popcosmos: Insights from generative modeling of a deep, infrared-selected galaxy population. *The Astrophysical Journal*, 993(2):240, November 2025. URL <http://dx.doi.org/10.3847/1538-4357/ae0936>.
- Toth, P., Rezende, D. J., Jaegle, A., Racanière, S., Botev, A., and Higgins, I. Hamiltonian generative networks. In Rush, A. (ed.), *8th International Conference on Learning Representations*, April 2020. URL <https://openreview.net/forum?id=HJenn6VFvB>.
- Vershynin, R. *High-Dimensional Probability: An Introduction with Applications in Data Science*. Cambridge Series in Statistical and Probabilistic Mathematics. Cambridge University Press, 2nd edition, November 2025. URL <https://www.math.uci.edu/~rvershyn/papers/HDP-book/HDP-2.pdf>.
- Vincent, P. A connection between score matching and denoising autoencoders. *Neural Computation*, 23(7):1661–1674, 2011. URL [https://doi.org/10.1162/NECO\\_a\\_00142](https://doi.org/10.1162/NECO_a_00142).
- Weaver, J. R., Kauffmann, O. B., Ilbert, O., McCracken, H. J., Moneti, A., Toft, S., Brammer, G., Shuntov, M., Davidzon, I., Hsieh, B. C., Laigle, C., Anastasiou, A., Jespersen, C. K., Vinther, J., Capak, P., Casey, C. M., McPartland, C. J. R., Milvang-Jensen, B., Mobasher, B., Sanders, D. B., Zalesky, L., Arnouts, S., Aussel, H., Dunlop, J. S., Faisst, A., Franx, M., Furtak, L. J., Fynbo, J. P. U., Gould, K. M. L., Greve, T. R., Gwyn, S., Kartaltepe, J. S., Kashino, D., Koekemoer, A. M., KokoREV, V., Le Fèvre, O., Lilly, S., Masters, D., Magdis, G.,

Mehta, V., Peng, Y., Riechers, D. A., Salvato, M., Sawicki, M., Scarlata, C., Scoville, N., Shirley, R., Silverman, J. D., Snepken, A., Smolčić, V., Steinhardt, C., Stern, D., Tanaka, M., Taniguchi, Y., Teplitz, H. I., Vaccari, M., Wang, W.-H., and Zamorani, G. COSMOS2020: A panchromatic view of the Universe to  $z \sim 10$  from two complementary catalogs. *The Astrophysical Journal Supplement Series*, 258(1):11, January 2022. URL <https://doi.org/10.3847/1538-4365/ac3078>.

Yang, L., Zhang, Z., Song, Y., Hong, S., Xu, R., Zhao, Y., Zhang, W., Cui, B., and Yang, M.-H. Diffusion models: A comprehensive survey of methods and applications. *ACM Computing Surveys*, 56(4):105, November 2023. URL <https://doi.org/10.1145/3626235>.

Yin, T., Gharbi, M., Zhang, R., Shechtman, E., Durand, F., Freeman, W. T., and Park, T. One-step diffusion with distribution matching distillation. In *2024 IEEE/CVF Conference on Computer Vision and Pattern Recognition (CVPR)*, pp. 6613–6623, 2024. URL <https://doi.org/10.1109/CVPR52733.2024.00632>.

Yun, T., Om, K., Lee, J., Yun, S., and Park, J. Posterior inference with diffusion models for high-dimensional black-box optimization. In Singh, A., Fazel, M., Hsu, D., Lacoste-Julien, S., Berkenkamp, F., Maharaj, T., Wagstaff, K., and Zhu, J. (eds.), *Proceedings of the 42nd International Conference on Machine Learning*, volume 267 of *Proceedings of Machine Learning Research*, pp. 73897–73917. PMLR, July 2025. URL <https://proceedings.mlr.press/v267/yun25a.html>.

Zheng, Q., Le, M., Shaul, N., Lipman, Y., Grover, A., and Chen, R. T. Q. Guided flows for generative modeling and decision making. *preprint*, November 2023. URL <https://arxiv.org/abs/2311.13443>.

Zhou, M., Zheng, H., Wang, Z., Yin, M., and Huang, H. Score identity distillation: Exponentially fast distillation of pretrained diffusion models for one-step generation. In Salakhutdinov, R., Kolter, Z., Heller, K., Weller, A., Oliver, N., Scarlett, J., and Berkenkamp, F. (eds.), *Proceedings of the 41st International Conference on Machine Learning*, volume 235 of *Proceedings of Machine Learning Research*, pp. 62307–62331. PMLR, July 2024. URL <https://proceedings.mlr.press/v235/zhou24x.html>.

Zhou, M., Gu, Y., Zheng, H., Song, L., He, G., Zhang, Y., Hu, W., and Yang, Y. Score distillation of flow matching models. *preprint*, September 2025. URL <https://arxiv.org/abs/2509.25127>.

## A. Stein class conditions

The boundary condition for the Stein class (Liu & Wang, 2016; Gorham & Mackey, 2017; Barp et al., 2019) sets the requirements on  $\mathbf{v}_t(\mathbf{x}_t)$  for Stein’s identity (6) to hold when applying the Langevin–Stein operator (5) to  $\mathbf{v}_t(\mathbf{x}_t)$ . The requirement can be expressed for  $\mathbf{x}_t \in \mathbb{R}^D$  (see e.g. Liu et al., 2016) as a vanishing boundary flux,

$$\lim_{R \rightarrow \infty} \oint_{\partial B_R} \langle p_t(\mathbf{x}_t) \mathbf{v}_t(\mathbf{x}_t), \hat{\mathbf{n}} \rangle dS \rightarrow 0, \quad (41)$$

where  $\hat{\mathbf{n}} = \mathbf{x}_t / \|\mathbf{x}_t\| \in \mathbb{R}^D$  is the outward unit normal to the ball  $B_R$  with  $R = \|\mathbf{x}_t\|$ , analogously to (18).

### A.1. Diffusion models

For diffusion models of the class considered by Song et al. (2021b),  $\mathbf{v}_t(\mathbf{x}_t) = \mathbf{f}(\mathbf{x}_t, t) - \frac{1}{2}g^2(t) \nabla \log p_t(\mathbf{x}_t)$ , which gives

$$\begin{aligned} p_t(\mathbf{x}_t) \mathbf{v}_t(\mathbf{x}_t) &= p_t(\mathbf{x}_t) \mathbf{f}(\mathbf{x}_t, t) - \frac{1}{2}g^2(t) \nabla p_t(\mathbf{x}_t) \\ &= \mathbb{E}_{\mathbf{x}_\varepsilon} \left[ p_t(\mathbf{x}_t | \mathbf{x}_\varepsilon) \mathbf{f}(\mathbf{x}_t, t) - \frac{1}{2}g^2(t) \nabla p_t(\mathbf{x}_t | \mathbf{x}_\varepsilon) \right], \end{aligned} \quad (42)$$

at the boundary. For the (sub-)VP-SDE, we have  $\mathbf{f}(\mathbf{x}_t, t) = -\frac{1}{2}\beta(t)\mathbf{x}_t$ , giving  $\langle \mathbf{f}(\mathbf{x}_t, t), \hat{\mathbf{n}} \rangle = -\frac{1}{2}\beta(t)$ , whilst for the variance exploding (VE)-SDE, we have  $\mathbf{f}(\mathbf{x}_t, t) = 0$ . The transition probabilities,  $p(\mathbf{x}_t | \mathbf{x}_\varepsilon)$  are Gaussian, with general form  $N(\nu(t)\mathbf{x}_\varepsilon, \eta^2(t)\mathbf{I})$ , where  $\nu(t)$  and  $\eta(t)$  are scalar-valued functions of  $t$ . This gives

$$\nabla p_t(\mathbf{x}_t | \mathbf{x}_\varepsilon) = -\frac{p(\mathbf{x}_t | \mathbf{x}_\varepsilon)}{\eta^2(t)} (\mathbf{x}_t - \nu(t)\mathbf{x}_\varepsilon), \quad (43)$$

and thus

$$\langle \nabla p_t(\mathbf{x}_t | \mathbf{x}_\varepsilon), \hat{\mathbf{n}} \rangle = -\frac{p(\mathbf{x}_t | \mathbf{x}_\varepsilon)}{\eta^2(t)} (1 - \nu(t) \langle \mathbf{x}_\varepsilon, \hat{\mathbf{n}} \rangle). \quad (44)$$

By Cauchy–Schwarz (see e.g. Vershynin, 2025), we can bound the inner product between  $\mathbf{x}_\varepsilon$  and the outward norm,  $|\langle \mathbf{x}_\varepsilon, \hat{\mathbf{n}} \rangle| \leq \|\mathbf{x}_\varepsilon\|$ . The terms in the integrand of (41) consequently take the form  $\mathbb{E}_{\mathbf{x}_\varepsilon} [p_t(\mathbf{x}_t | \mathbf{x}_\varepsilon)]$ , or can be upper-bounded by  $\mathbb{E}_{\mathbf{x}_\varepsilon} [p_t(\mathbf{x}_t | \mathbf{x}_\varepsilon) \|\mathbf{x}_\varepsilon\|]$ , up to  $t$ -dependent constants. Transforming to hyper-spherical coordinates (e.g. Song & Ermon, 2020), we have

$$\begin{aligned} p_t(\mathbf{x}_t | \mathbf{x}_\varepsilon) &\propto R^{D-1} \exp\left(\frac{-\|\mathbf{x}_t - \nu(t)\mathbf{x}_\varepsilon\|^2}{2\eta^2(t)}\right) \\ &\leq R^{D-1} \exp\left(\frac{-(R - \nu(t)\|\mathbf{x}_\varepsilon\|)^2}{2\eta^2(t)}\right), \end{aligned} \quad (45)$$

by the reverse triangle inequality for  $\|\mathbf{x}_t - \nu(t)\mathbf{x}_\varepsilon\|$ . If  $\|\mathbf{x}_\varepsilon\| < \infty \forall \mathbf{x}_\varepsilon$ ,  $p(\mathbf{x}_t | \mathbf{x}_\varepsilon)$  and  $\|\mathbf{x}_\varepsilon\| p(\mathbf{x}_t | \mathbf{x}_\varepsilon)$  will vanish

as  $R \rightarrow \infty$ , meaning the expectation over  $\mathbf{x}_\varepsilon$ , and the full surface integral in (41) will also vanish. We therefore expect that for VE-, VP-, and sub-VP-SDEs, and a well behaved target distribution, the vector field produced by a diffusion model should be Stein class  $\forall t \geq \varepsilon$ .

## A.2. Flow-matching models

For flow-matching models (and related classes like TrigFlow that obey a similar noising schedule), we have

$$p(\mathbf{x}_t)\mathbf{v}_t(\mathbf{x}_t) = \mathbb{E}_{\mathbf{x}_\varepsilon} [p(\mathbf{x}_t|\mathbf{x}_\varepsilon)\mathbf{v}_t(\mathbf{x}_t)], \quad (46)$$

with the distribution of  $\mathbf{x}_t$  being Gaussian conditional on  $\mathbf{x}_\varepsilon$  per (30). Using the spherical coordinate transform as in Song & Ermon (2020), we can re-write the conditional distribution of  $\mathbf{x}_t$  as

$$\begin{aligned} p(\mathbf{x}_t|\mathbf{x}_\varepsilon) &\propto R^{D-1} \exp\left(\frac{-\|\mathbf{x}_t - \alpha_t \mathbf{x}_\varepsilon\|^2}{2\sigma_t^2}\right) \\ &\leq R^{D-1} \exp\left(\frac{-(R - \alpha_t \|\mathbf{x}_\varepsilon\|)^2}{2\sigma_t^2}\right), \end{aligned} \quad (47)$$

where we have used the reverse triangle inequality to lower-bound  $\|\mathbf{x}_t - \alpha_t \mathbf{x}_\varepsilon\|^2$  as in (45). By Cauchy–Schwarz, we can bound  $|\langle \mathbf{v}_t(\mathbf{x}_t), \hat{\mathbf{n}} \rangle| \leq \|\mathbf{v}_t(\mathbf{x}_t)\|$  as being less than or equal to the magnitude of the learned vector field. If  $\|\mathbf{v}_t(\mathbf{x}_t)\|$  is bounded  $\forall \mathbf{x}_t$ , or is limited to polynomial growth with  $R$ , the integrand in (41) will vanish  $\forall \mathbf{x}_\varepsilon$  and the Stein class will be satisfied (c.f. also the conditions discussed in §3.1 and §3.3).

## B. Comparison of trace estimators

As a cross-check of our main results (§4), we perform some simple experiments to test the scaling and performance of the stochastic trace estimators on randomly generated matrices. To test the algorithms on non-PSD matrices, we generate a random  $D \times D$  matrix  $\mathbf{A}$  with  $A_{ij} \sim N(0, 1)$  for  $D = 4, 16, 64, 256$ . To test performance on PSD matrices we take  $A_{ij} \sim \text{Half-}N(0, 1)$ .

We compute the exact trace  $\text{Tr}(\mathbf{A}) = \sum_{i=1}^D A_{ii}$ , and compare this to the trace computed using the stochastic estimators. We average over  $B = 65536, 16384, 4096, 1024$  random matrices for a given  $D$  to calculate the MAE relative to the exact trace. For the Hutchinson estimator, we use  $n \in [1, 512]$  probe vectors, requiring  $m = n$  matrix–vector multiplications for a given  $n$ . For Hutch++ and XTrace, we use  $n \in [1, D]$  probe vectors with a rank- $n$  QR decomposition, requiring respectively  $m = 3n$  or  $m = 2n$  matrix–vector multiplications.

Figure 6 shows the results of our experiment. For the PSD case, shown in the top panel, we see that Hutch++ and XTrace outperform Hutchinson for all  $m \geq 4$  irrespective

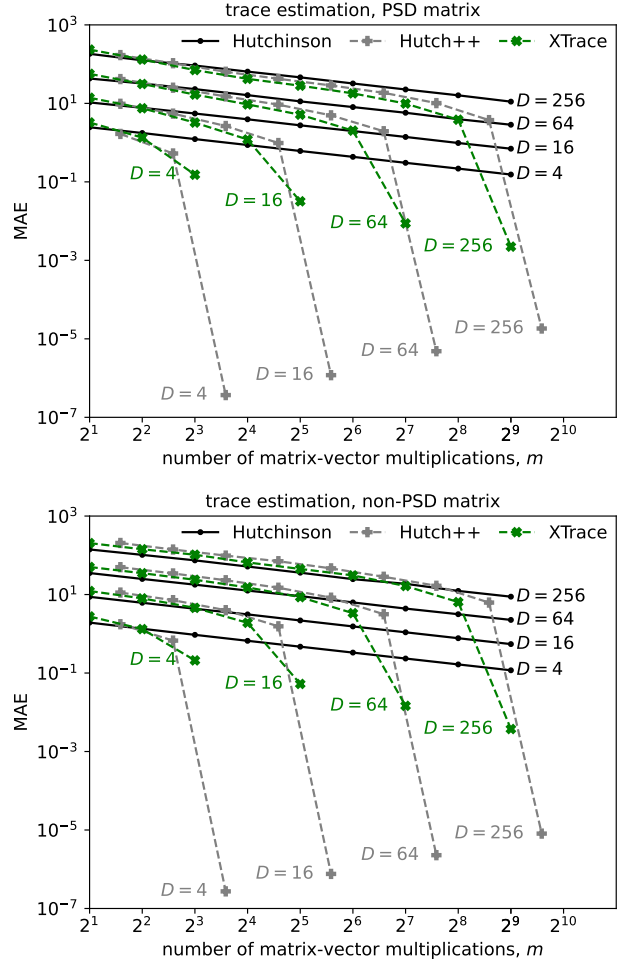


Figure 6. Stochastic trace estimation for a randomly generated  $D \times D$  matrix  $\mathbf{A}$ . *Top*: PSD  $\mathbf{A}$  with  $A_{ij} \sim \text{Half-}N(0, 1)$ . *Bottom*: non-PSD  $\mathbf{A}$  with  $A_{ij} \sim N(0, 1)$ . MAE relative to exact trace is calculated by averaging over  $B = 65536, 16384, 4096, 1024$  matrices for  $D = 4, 16, 64, 256$ .

Table 4. Training cost for *StAD* compared to directly learning the divergence—H(1) or the residual—H(1)+B. Cache time covers the generation of targets (vector field evaluations for *StAD*, divergence or residual estimates for H(1) or H(1)+B. Train time covers the training of the distillation network using the cached targets. Step time covers a single training epoch.

method	cache (s)	train (s)	total (s)	step (s)
H(1)	172.9	7770.5	7943	0.03
H(1)+B	172.9	7780.1	7953	0.03
<i>StAD</i>	73.1	7780.6	7854	0.16

Table 5. Comparing *StAD* to directly learning the divergence—H(1) or the residual—H(1)+B. We use the same FiLM-CNN described in Table 10. MAE is computed against log probabilities summed over 256 images with H(16). JVPs are per-target evaluation.

method	JVP	steps	time (s)	MAE	mean $\pm$ std
H(1)	1	281091	7943	0.59	0.58 $\pm$ 0.33
H(1)+B	1	279727	7953	0.35	0.35 $\pm$ 0.22
<i>StAD</i>	0	50000	7854	0.24	0.21 $\pm$ 0.26

of  $D$ , with XTrace being the most performant algorithm at fixed  $m$ . For the non-PSD case, the result is more dependent on  $D$  and  $m$ . For  $m \ll D$ , the basic Hutchinson estimator tends to yield a lower MAE, as seen in many of our main experiments (§4). We find that XTrace begins outperforming Hutchinson at lower  $m$  than Hutch++ does, and consistently outperforms Hutch++ to a similar level as in the PSD case. We find that for  $m \geq D$  (i.e.  $n \geq D/2$ ) XTrace consistently yields a lower MAE than the basic Hutchinson estimator, with parity achieved at  $m = D/2$  (i.e.  $n = D/4$ ). For PSD and non-PSD matrices, we find that Hutch++ always converges to a very small MAE at  $n = D$ , aligning with the findings of Meyer et al. (2021) who prove that their estimator will always asymptotically beat Hutchinson.

### C. Direct divergence regression

*StAD* avoids computing the Jacobian or its trace in the definition of its loss. However, directly regressing against divergence estimates from trace estimators (analogously to e.g. Ai et al., 2026) could be a viable alternative. To study how *StAD* compares to directly learning the divergence or the residual (defined in Equation 13), we train a neural network to regress against divergence estimates from Hutchinson, denoted as H(1), or against residual estimates, denoted as H(1)+B. The computational cost of training the direct divergence regressors are given Table 4, with the log probability accuracy compared to *StAD* in Table 5.

In Table 4, we report the time taken to build up a cache of targets (either vector field evaluations for *StAD*, or divergence/residual estimates for the direct regressors), the training time, the total compute time (training + cache), and the time taken per training epoch. We find that *StAD*

takes more seconds per epoch compared to directly learning the divergence. Hence, to maintain a fair comparison we match the wall-clock time across methods and find that for a comparable time budget *StAD* achieves better MAE than learning the divergence or the residual directly. A natural objection is that averaging over  $N > 1$  Hutchinson probes would reduce target variance and achieve better results. However, this would scale cache cost linearly while reducing target noise only by  $\sqrt{N}$ , rapidly exceeding *StAD*’s total cost without closing the accuracy gap.

### D. Time sampling

The time averaged objective functions for *StAD* are computed by averaging over uniformly sampled times,  $t \sim U(\varepsilon, T)$ . This has the desirable property of weighting all time-steps equally in the total loss. However, our experiments showed that oversampling times closer to  $\varepsilon$  (i.e. closer to the target distribution) produces empirically better results, with lower variance in the resulting trace estimator. This is likely due to the behaviour of the vector field becoming less complex as  $t \rightarrow T$ .

To achieve the benefit of denser early-time sampling, without changing the meaning of the time-integrated loss, we use an importance re-weighting trick, similar to Song et al. (2021a). We define a new proposal distribution,  $q(t) \propto 1/t^2$  for  $t \in [\varepsilon, T]$ :

$$q(t) = \begin{cases} t^{-2}(1/\varepsilon - 1/T)^{-1}; & \text{if } \varepsilon \leq t \leq T \\ 0; & \text{otherwise.} \end{cases} \quad (48)$$

We rewrite our old loss function as an expectation over  $q(t)$ , re-weighted by  $w(t) = p(t)/q(t) \propto t^2$ . This gives us

$$\begin{aligned} L(\delta) &= \mathbb{E}_{t \sim p(t)} [L(\delta; t)] = \int_{\varepsilon}^T p(t) L(\delta; t) dt \\ &\propto \int_{\varepsilon}^T q(t) t^2 L(\delta; t) dt = \mathbb{E}_{t \sim q(t)} [t^2 L(\delta; t)], \end{aligned} \quad (49)$$

which we use as our objective for the experiments in §4.

### E. Extension to TrigFlow

Flow-map models (Sabour et al., 2025) have been introduced to unify recent frameworks, such as consistency models (Song et al., 2023; Song & Dhariwal, 2024; Lu & Song, 2025) and mean flow (Geng et al., 2025), that were developed for faster sampling under diffusion and flow-based models. Of these formulations, the TrigFlow continuous-time consistency model (Lu & Song, 2025) is a particularly natural fit for *StAD*.

Lu & Song (2025) introduce TrigFlow, that optimises the objective

$$\mathcal{L}(\theta) = \mathbb{E}_t \mathbb{E}_{\mathbf{x}_\varepsilon} \mathbb{E}_{\mathbf{x}_t | \mathbf{x}_\varepsilon} \left[ \left\| \sigma_d \mathbf{v}_t(\mathbf{x}_t; \theta) - \mathbf{u}_t \right\|^2 \right] \quad (50)$$

where  $\sigma_d$  is the variance in the data distribution, and  $\mathbf{v}_t(\mathbf{x}_t; \theta)$  is a model vector field with parameters  $\theta$ . Here, the noising schedule is defined by  $\mathbf{x}_t = \cos(t)\mathbf{x}_\varepsilon + \sin(t)\mathbf{z}$  with  $p(\mathbf{z}) = N(0, \sigma_d^2 \mathbf{I})$ , equivalent to the flow-matching noise schedule (30) with  $\alpha_t = \cos(t)$  and  $\sigma_t = \sigma_d \sin(t)$ . Thus the flow matching objective’s target can be defined as  $\mathbf{u}_t := -\sin(t)\mathbf{x}_\varepsilon + \cos(t)\mathbf{z}$ , giving us

$$\mathbf{x}_\varepsilon = \cos(t)\mathbf{x}_t - \sin(t)\mathbf{u}_t. \quad (51)$$

The conditional expectation as shown by Zhou et al. (2025) is  $\mathbb{E}[\mathbf{x}_\varepsilon | \mathbf{x}_t] = \cos(t)\mathbf{x}_t - \sin(t)\mathbb{E}[\mathbf{u}_t | \mathbf{x}_t]$ , under the flow-matching regression objective  $\mathbf{v}_t(\mathbf{x}_t) \approx \mathbb{E}[\mathbf{u}_t | \mathbf{x}_t]$ . Now, using (29), we can derive the score for TrigFlow models under Gaussian assumptions as:

$$\mathbf{s}_t(\mathbf{x}_t) = -\frac{\mathbf{x}_t - \cos(t)\mathbb{E}[\mathbf{x}_\varepsilon | \mathbf{x}_t]}{\sin^2(t)} \quad (52)$$

Using the trigonometric path relation gives us:

$$\begin{aligned} \mathbf{s}_t(\mathbf{x}_t) &\approx -\frac{\mathbf{x}_t - \cos(t) (\cos(t)\mathbf{x}_t - \sin(t)\mathbf{v}_t(\mathbf{x}_t))}{\sin^2(t)} \\ &\approx -(\mathbf{x}_t + \cot(t)\mathbf{v}_t(\mathbf{x}_t)) \end{aligned} \quad (53)$$

This allows us to define the baseline,

$$b_t(\mathbf{x}_t) = \langle \mathbf{v}_t(\mathbf{x}_t), \mathbf{x}_t \rangle + \cot(t) \|\mathbf{v}_t(\mathbf{x}_t)\|^2 \quad (54)$$

and the residual,

$$r_t(\mathbf{x}_t) = \langle \nabla, \mathbf{v}(\mathbf{x}_t) \rangle - \langle \mathbf{v}_t(\mathbf{x}_t), \mathbf{x}_t \rangle - \cot(t) \|\mathbf{v}_t(\mathbf{x}_t)\|^2. \quad (55)$$

Similarly to flow-matching (§3.2), the rest of the StAD objective remains the same. This allows us to approximate the divergence and compute log-likelihood cheaply for consistency models.

## F. Experiment details

### F.1. Hardware

All of the experiments conducted here were run on NVIDIA-A100 GPUs with 40GiB VRAM and 1TB of RAM on 48 core nodes. Each node utilised a  $2 \times 24$  Core AMD EPYC 7402 2.8 GHz processor.

### F.2. Software

We use the `torchdiffeq` (Chen et al., 2018a) library for all the experiments, with the `dopri5` adaptive Runge-Kutta ODE solver (Dormand & Prince, 1980). We set the absolute and relative tolerances to  $10^{-5}$  for our solvers for StAD, the stochastic estimators, and the exact trace. All code is implemented in PyTorch (Paszke et al., 2019).

### F.3. StAD implementation

We describe the StAD distillation procedure for diffusion in Algorithm 1, for the flow-matching case the algorithm stays the same, but we build the cache not from SDE marginals, but by evaluating the teacher velocity at  $\mathbf{x}_t$ .

---

**Algorithm 1** Cached Stein distillation for conditional diffusion (StAD implementation)

---

**Require:** data samples and contexts  $\{(\mathbf{x}_\varepsilon, c)\}$ ; teacher PF-ODE drift  $\mathbf{v}_\theta(\mathbf{x}_t; t, c)$ ; scalar head  $\delta_\phi(\mathbf{x}_t; t, c)$ ; SDE conditional mean, variance  $\nu(t), \eta^2(t)$ .

**Require:** proposal  $q(t)$ ; target  $p(t) = U(\varepsilon, t)$ ; cache size  $M$ ; steps  $S$ ; batch size  $B$ ; rebuild period  $K$ ; regularization  $\kappa_R(\|\mathbf{x}_t\|)$ ;  $L^2$  penalty  $l$ .

- 1: build cache  $\mathcal{C} = \{(\mathbf{x}_t, t, \mathbf{v}_t, c)\}_{m=1}^M$ :
- 2: **for**  $m = 1 \dots M$  **do**
- 3:   sample  $(\mathbf{x}_\varepsilon, c) \sim$  data
- 4:   normalize  $\mathbf{x}_\varepsilon \leftarrow (\mathbf{x}_\varepsilon - \text{shift})/\text{scale}$ ;  $c$  if used
- 5:   sample  $t \sim q(t)$ ,  $\mathbf{z} \sim \mathcal{N}(0, \mathbf{I})$
- 6:    $\mathbf{x}_t \leftarrow \nu_t(\mathbf{x}_\varepsilon) + \eta(t)\mathbf{z}$
- 7:    $\mathbf{v}_t \leftarrow \mathbf{v}_\theta(\mathbf{x}_t; t, c)$
- 8:   store  $(\mathbf{x}_t, t, \mathbf{v}_t, c)$  in  $\mathcal{C}$
- 9: **end for**
- 10: **for**  $s = 1 \dots S$  **do**
- 11:   sample  $\{(\mathbf{x}_i, t_i, \mathbf{v}_i, c_i)\}_{i=1}^B$  uniformly from  $\mathcal{C}$
- 12:    $w_i \leftarrow p(t_i)/q(t_i)$
- 13:    $\lambda_i \leftarrow \kappa_R(\|\mathbf{x}_i\|)$
- 14:    $\delta_i \leftarrow \lambda_i \delta_\phi(\mathbf{x}_i; t_i, c_i)$
- 15:    $\mathbf{g}_i \leftarrow \nabla_{\mathbf{x}_i} \delta_i$
- 16:    $\mathcal{L} \leftarrow \frac{1}{B} \sum_{i=1}^B w_i \left( \delta_i^2 + 2\langle \mathbf{g}_i, \mathbf{v}_i \rangle + l\|\mathbf{g}_i\|^2 \right)$
- 17:   update  $\phi$  using  $\nabla_\phi \mathcal{L}$
- 18:   **if**  $K > 0$  **and**  $s \bmod K = 0$  **then**
- 19:     rebuild  $\mathcal{C}$  as above
- 20:   **end if**
- 21: **end for**

---

### F.4. $\delta$ regularisation

For most of our experiments we set  $R$  as a high quantile of  $\|\mathbf{x}\|$ . For the astrophysical flux, ImageNet-32x32 and CIFAR-10 experiments, we set  $R$  to the 99.5th percentile of  $\|\mathbf{x}\|$ . We generally follow the cosine function defined in §3.3. However we can also make harder constraints on  $\delta$  by using a bump function, where,  $\kappa_R \propto \exp(1/\|\mathbf{x}\|^2)$  if  $R < \|\mathbf{x}\| < 2R$ .

### F.5. Hyperparameters

#### F.5.1. ASTROPHYSICAL FLUXES

**Training** We describe the hyperparameters used to train the diffusion model to predict astrophysical flux uncertainties in Table 6. We use tanh activation functions for the MLP

Table 6. Diffusion model hyperparameters for flux uncertainty prediction in the COSMOS2020 dataset.

SDE	$\beta_{\max}$	epochs	LR	optimiser
VP	20	1000	step; 1e-4 to 1e-5	Adam

Table 7. MLP head,  $\delta$ , for the VP-SDE diffusion model trained on COSMOS2020. We set  $R$  to the  $P_R$ th percentile of  $\|\mathbf{x}\|$ .

MLP	$P_R$	epochs	LR	optimiser
$512 \times 3$	99.5%	$1 \times 10^5$	1e-4 to 1e-8	Adam

and employ a step scheduler with the step size of half the learning rate, alongside with a heating step schedule of  $2 \times$  the batch size, starting with 64.

**Distilling** We describe the hyperparameters used to distill the astrophysical model in Table 7. We use a cosine scheduler for the learning rate. Each epoch is extremely efficient; we observe wall-clock of  $\sim 1.5$  hours to achieve the accuracy showed in Figure 2 on the hardware specified in Appendix F.1.

#### F.5.2. IMAGENET-32x32 AND CIFAR-10

**Training** We train a U-Net architecture, whose hyperparameters are listed in Table 8 and Table 9, respectively for CIFAR and ImageNet-32x32 models.

**Distilling** We distill the PF-ODEs learned by these models, using a compact CNN architecture, with FiLM conditioning for injecting time into data. Hyperparameters and further architectural details for the distillation head are described in Table 10 for CIFAR-10 and in Table 11 for ImageNet-32x32.

#### F.6. Stochastic trace estimators

We use Rademacher distributed test vectors for all our Hutchinson tests. We base our implementation of Hutch++, including caching of the  $QR$  decomposition, on Liu et al. (2025). We update the cached  $\mathbf{Q}$  matrices once per Runge-Kutta step (i.e. every sixth function evaluation for the `dopri5` solver). Our implementation of XTrace is based in the efficient algorithm described in the supplementary material of Epperly et al. (2024).

### G. Further ImageNet and CIFAR-10 results

In Figure 7 we show the correlation between NLLs from the Hutchinson (2-probe) estimator and *StAD* for 2048 samples from CIFAR-10. In Figure 8 we compare NLL histograms from *StAD* and Hutchinson for ImageNet-32x32.

Table 8. Training hyperparameters for CIFAR-10.

hyperparameter	value
SDE	VP-SDE
loss	denoising score matching
base channels	128
channel multipliers	(1, 2, 2, 2)
ResBlocks per level	2
attention resolutions	16, 8
attention heads	4
optimizer	AdamW
learning rate	$2 \times 10^{-4}$
batch size	256
epochs	400
gradient clipping	1.0
EMA decay	0.999
sampling steps	200

Table 9. Training hyperparameters for ImageNet-32x32.

hyperparameter	value
SDE	VP-SDE
loss	denoising score matching
base channels	128
channel multipliers	(1, 2, 2, 2)
ResBlocks per level	2
attention resolutions	16, 8
attention heads	4
optimizer	AdamW
learning rate	$2 \times 10^{-4}$
batch size	256
epochs	200
gradient clipping	1.0
EMA decay	0.999
sampling steps	200

Table 10. Distillation hyperparameters for CIFAR-10  $\delta$ -head.

hyperparameter	value
<i>architecture</i>	
head type	FiLM-CNN
base channels	64
time embedding dim	256
group norm groups	16
time input	$\log t$
downsampling	$32 \rightarrow 16 \rightarrow 8$ (stride-2 convs)
output	global pool $\rightarrow$ MLP $\rightarrow$ scalar
<i>training</i>	
optimizer	AdamW
learning rate	$1 \times 10^{-4}$
training steps	600,000
batch size	2,048
gradient clipping	1.0
<i>caching</i>	
cache samples	262,144
cache refresh interval	2,000 steps
time sampler	uniform
<i>cutoff</i>	
cutoff mode	cosine
$P_R$	99.5%

Table 11. Distillation hyperparameters for ImageNet-32x32.

hyperparameter	value
<i>architecture</i>	
head type	FiLM-CNN
base channels	64
time embedding dim	256
group norm groups	16
time input	$\log t$
downsampling	$32 \rightarrow 16 \rightarrow 8$ (stride-2 convs)
output	global pool $\rightarrow$ MLP $\rightarrow$ scalar
<i>training</i>	
optimizer	AdamW
learning rate	$1 \times 10^{-4}$
training steps	600,000
batch size	2,048
gradient clipping	1.0
directional method	exact gradient (autograd)
<i>caching</i>	
cache samples	262,144
cache refresh interval	2,000 steps
time sampler	uniform
<i>cutoff</i>	
cutoff mode	cosine
$P_R$	99.5%

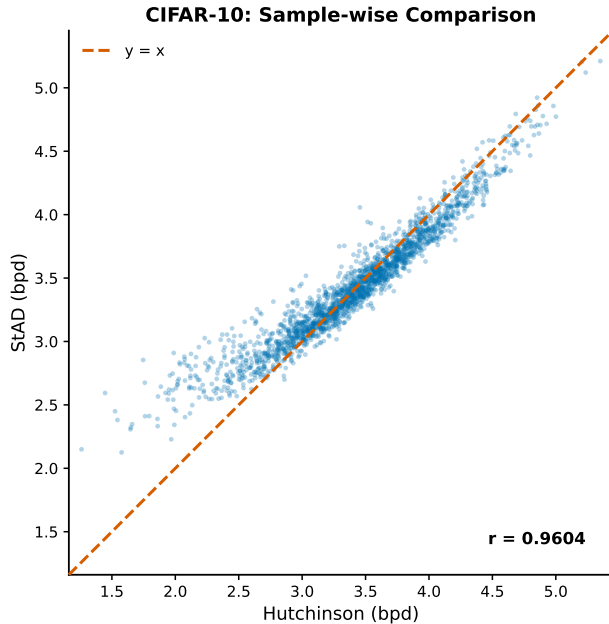


Figure 7. Image-wise NLL comparison (StAD vs. Hutchinson with 2 probes) for 2048 images from CIFAR-10.

## H. CIFAR-10 and ImageNet samples

In Figure 9 and Figure 10, we show example images generated by our teacher diffusion models (in both cases based on a VP-SDE and U-Net score network) for the CIFAR-10 and ImageNet-32x32 training datasets.

Likelihood Comparison: ImageNet32

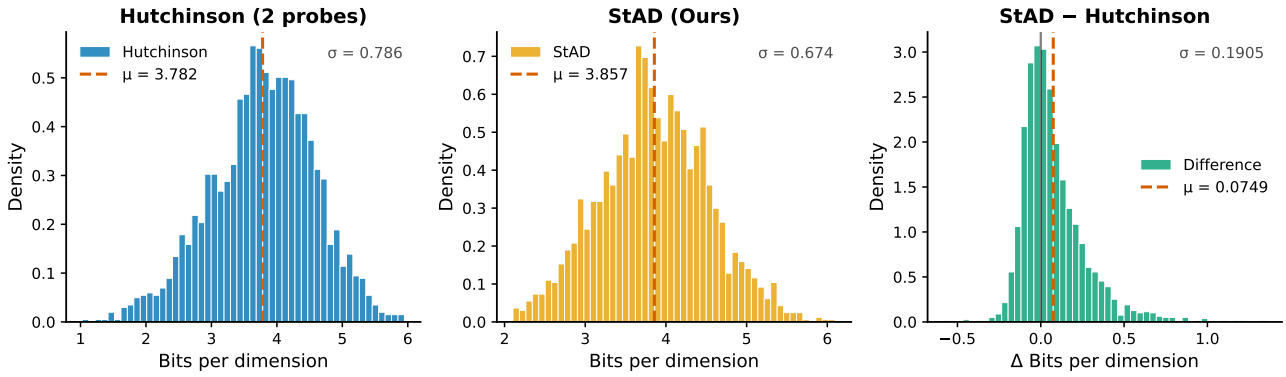


Figure 8. NLL histograms for 2048 images from ImageNet-32x32. *Left*: Using the Hutchinson algorithm with 2 probes to estimate the NLL. *Centre*: Using *StAD*. *Right*: Difference between *StAD* and Hutchinson:  $NLL[StAD] - NLL[Hutchinson]$ .

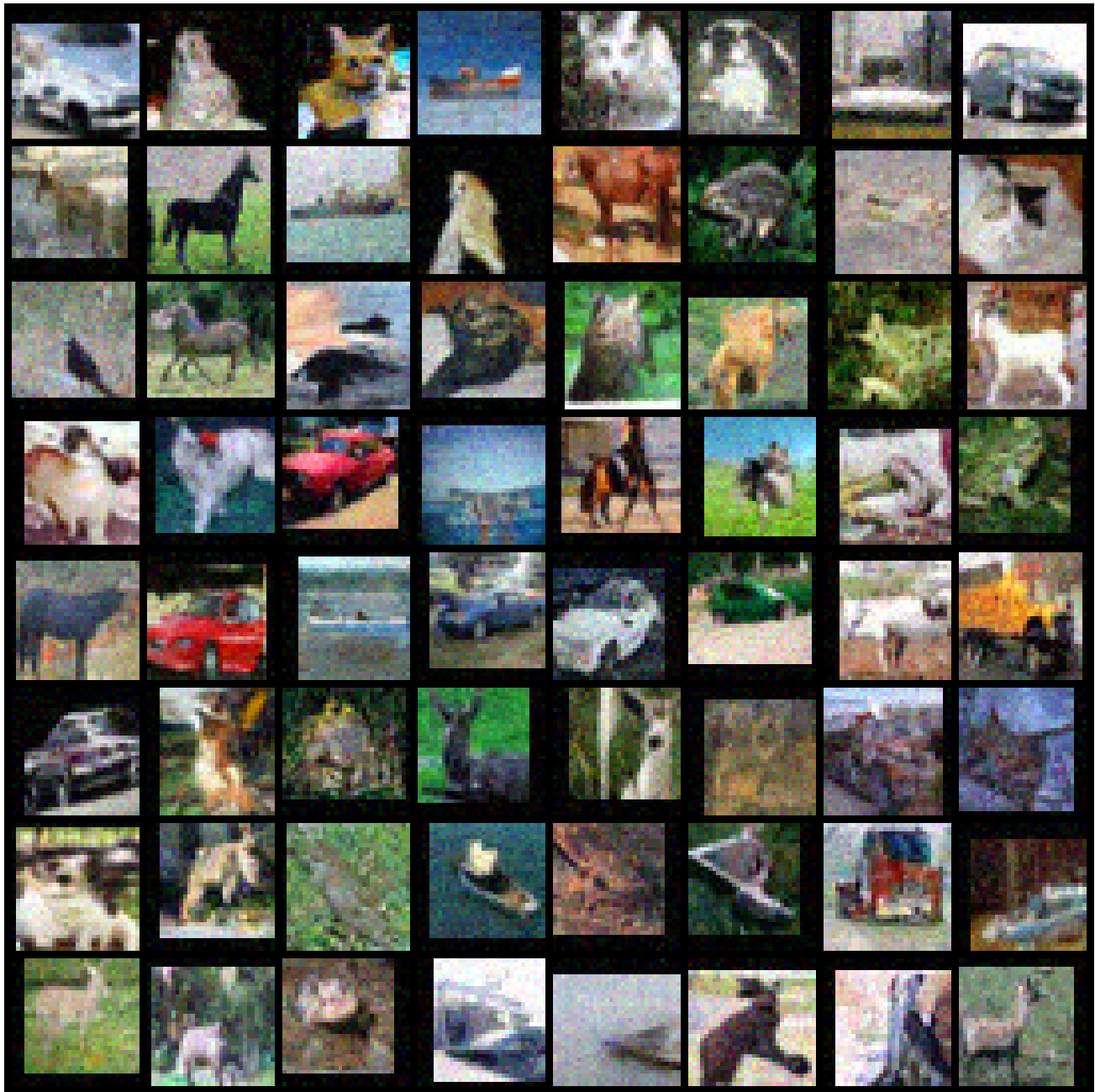


Figure 9. Unconditional CIFAR-10 samples from a VP-SDE diffusion model trained with a U-Net architecture.



Figure 10. ImageNet-32x32 samples from a VP-SDE diffusion model trained with a U-Net architecture.